A glial ClC Cl− channel mediates nose touch responses in C. elegans

DOI: http://doi.org/10.1016/j.neuron.2021.11.010

Published in final edited form as:
Neuron. 2022 February 02; 110(3): 470–485.e7. doi:10.1016/j.neuron.2021.11.010.

A glial ClC Cl^- channel mediates nose touch responses in *C. elegans*

Jesus Fernandez-Abascal, **Christina K. Johnson**, **Bianca Graziano**, **Lei Wang**, **Nicole Encalada**, **Laura Bianchi**[*]
Department of Physiology and Biophysics, Miller School of Medicine, University of Miami, Florida, 33136, USA.

SUMMARY

In touch receptors, glia and accessory cells play a key role in mechanosensation. However, the mechanisms underlying such regulation are poorly understood. We show for the first time that chloride channel CLH-1 is needed in glia of *C. elegans* nose touch receptors for touch responses and for regulation of excitability. Using *in vivo* Ca^{2+} and Cl^- imaging, behavioral assays, and combined genetic and pharmacological manipulations, we show that CLH-1 mediates Cl^- flux needed for glial GABA inhibition of ASH sensory neurons' function and for regulation of cAMP levels in ASH neurons. Finally, we show that rat ClC-2 channel rescues *clh-1*'s nose touch insensitive phenotype, underscoring conservation of function across species. Our work identifies a glial Cl^- channel as a novel regulator of touch sensitivity. We propose that glial CLH-1 regulates the interplay between Ca^{2+} and cAMP signaling in ASH neurons to control the sensitivity of the worm's nose touch receptors.

Graphical Abstract

[*]Lead contact: Laura Bianchi (lbianchi@med.miami.edu).

AUTHOR CONTRIBUTIONS

L. B. designed the research and wrote the manuscript. J. F. A. designed the research, performed the experiments, and wrote the manuscript. C. K. J., B. G., L. W., and N. E., performed experiments. All authors have read, commented, and accepted the manuscript. CKJ current affiliation: Wake Forest School of Medicine.

DECLARATION OF INTERESTS

The authors declare no competing interests.

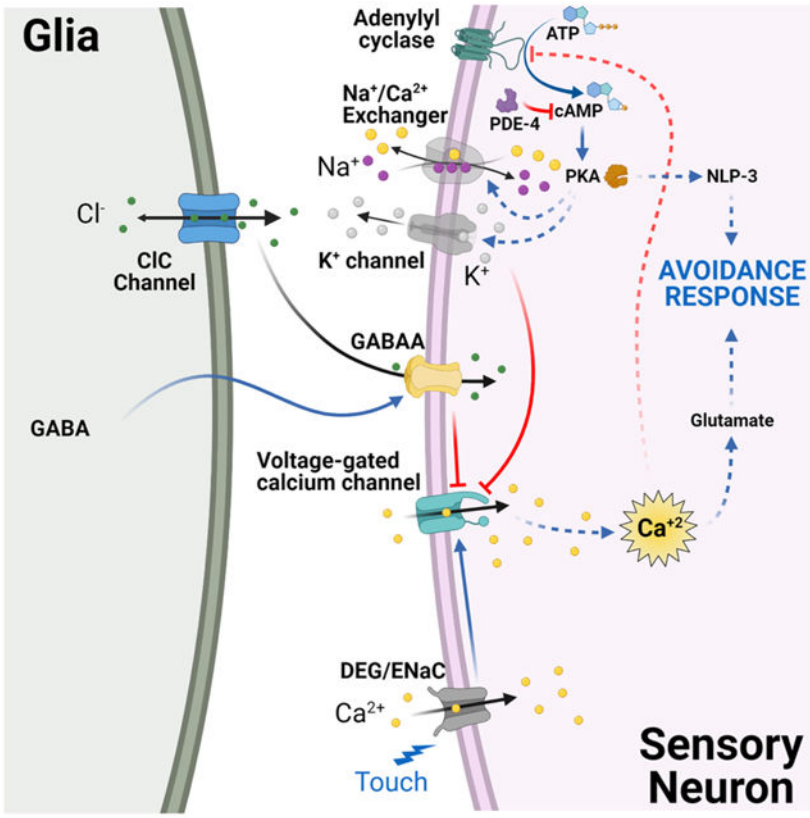

In Brief

Fernandez-Abascal et al. report that a ClC Cl^- channel expressed in glia associated with mechanosensory neurons mediates touch responses. The glial Cl^- channel mediates efflux of Cl^- from glia which consequently permeates through GABA receptors expressed on mechanosensory neurons resulting in regulation of neuronal Ca^{2+} and cAMP levels enabling touch responses.

INTRODUCTION

Touch is the least understood of the senses, yet it is vital for our survival. The study of touch has historically focused on understanding how mechanical forces are sensed by the mechanosensory neurons. However, touch receptors are composed of both neuronal endings and accessory cells, including glia. While the understanding of the contribution of accessory cells to touch is at its infancy, studies in Merkel cells receptors have shown that Merkel cells, the non-neuronal components of these touch receptors, express mechano-sensitive channel piezo2, and are both necessary and sufficient to evoke firing of the αβ low threshold mechanosensors of the Merkel cell-neurite complex (Ikeda et al., 2014, Woo et al., 2014). Less is known about the contribution of lamellar cells of Schwann origin to the function of Pacinian and Meissner's corpuscles. However, two main functions have been suggested: modulation of nerve fiber excitability and detection of mechanical forces. Indeed, recent work using electrophysiological approaches on these corpuscles isolated from the duck’s bill has shown that the lamellar cells express mechanosensitive channels, and at least those of the Meissner's corpuscles express voltage-gated ion channels. These results raise the possibility that non-neuronal cells in these mechanoreceptors directly participate in sensory transduction (Nikolaev et al., 2020). Moreover, Pawson and colleagues had shown in the Pacinian corpuscles isolated from the cat, that GABA released by the lamellar cells inhibits action potential firing in the sensory neuron during the static portion of sustained pressure (Pawson et al., 2009). While these studies underscore the crucial role of accessory cells of mechanoreceptors in touch, molecular analyses in these less genetically-amenable systems have lagged behind.

In *C. elegans*, 25 of the 45 touch neurons are associated with glial sheath and socket cells (Altun and Hall, 2010, Goodman and Sengupta, 2019). Sheath and socket glia are needed for the function of the sensory neurons they surround, including the function of nose touch sensing neurons (Bacaj et al., 2008, Wang et al., 2008, Wang et al., 2012, Han et al., 2013, Singhvi et al., 2016, Johnson et al., 2020). The ClC chloride channel CLH-1 is an inwardly rectifying channel expressed in amphid sheath glia (AMsh glia) where it is needed for pH regulation (Grant et al., 2015). The CLH-1 mammalian homolog ClC-2 is also expressed in glia, including astrocytes and oligodendrocytes, where it has been proposed to regulate ionic homeostasis, including regulation of pH (Blanz et al., 2007, Depienne et al., 2013). Regulation of Cl^- homeostasis by glial ClC-2 might be important for GABA signaling. In support of this idea, Sik and colleagues showed that ClC-2 is localized in astrocytic endfeet that ensheath capillaries and blood vessels and in the neuropil of the stratum pyramidale in close proximity to GABAergic neurons (Sik et al., 2000). We thus hypothesized that CLH-1 might be needed for Cl^- homeostasis in the nematode amphid sensory organ and that its knockout may lead to sensory deficits. Using genetic and pharmacological approaches, we assayed glial and neuronal function, as well as behavioral nose touch responses, and found that glial CLH-1 is a key regulator of mechanosensory neuron ASH responses to touch. In particular, we show that CLH-1 is needed for GABA modulation of ASH excitability and for maintenance of Ca^{2+} and cAMP levels in these neurons. Our work sheds new light on the essential participation of touch receptors’ glial cells to sensory transduction and adds to our understanding of ion channels and intracellular cascades involved in transducing mechanical forces.

RESULTS

Cl^- channel CLH-1 is needed in amphid glia for nose touch response.

The voltage-gated chloride channel CLH-1 is enriched in the AMsh glia of the amphid sensory apparatus, where it is involved in pH regulation (Grant et al., 2015). Moreover, CLH-1 is needed in ASER neurons for experience-dependent chemotaxis to salt (Park et al., 2021). Thus, we hypothesized that this chloride channel may function in other sensory behaviors. CLH-1 might be well positioned to influence the function of sensory neurons by being localized where AMsh glia wrap around the cilia of sensory neurons. Therefore, we first analyzed the subcellular localization of CLH-1 in the AMsh glia using a genetically modified CRISPR-*cas9* strain expressing endogenous GFP tagged CLH-1. As shown in Fig. 1A, we found that CLH-1 was enriched at the tip of the AMsh glia process, where the cilia of sensory neurons are localized. Hence, we analyzed the response of *clh-1(ok658)* knockout worms to several sensory cues (Fig. 1B-D and Fig. S1A-C). We found that *clh-1* knockout worms have significantly reduced response to nose touch (Fig. 1B, 30.8 ± 1.3% versus 79.9 ± 0.9% in wild type). Nose touch avoidance behavior in *C. elegans* is mediated by a group of sensory neurons located in the head of the worm (Schafer, 2015). AMsh glia wrap around the sensory endings of only one set of these neurons, the polymodal ASH neurons (Kaplan and Horvitz, 1993). These neurons also mediate aversive response to octanol and high osmolarity (Bargmann et al., 1990). Interestingly though, we found that *clh-1* knockout animals respond normally to high osmolarity solutions and to octanol (Fig. 1C and 1D, respectively). Similarly, attraction to isoamyl alcohol, Na^+, and diacetyl was normal in *clh-1* knockout animals (Fig. S1A-C).

To confirm that *clh-1* is needed in AMsh glia for nose touch avoidance behavior, we knocked down *clh-1* in these glial cells by cell-specific RNAi expressed from the AMsh glia specific promoter T02B11.3 (Bacaj et al., 2008). We found that AMsh glia *clh-1* RNAi worms were also nose touch insensitive (Fig. 1B). Furthermore, expression of CLH-1 cDNA in AMsh glia using the T02B11.3 promoter or the *vap-1* promoter, known also to function in AMsh glia (Perens and Shaham, 2005), fully rescues nose touch insensitivity. In contrast, knockdown of *clh-1* in ASH under the control of the ASH specific promoter *sra-6* does not impair nose touch responses and expression of CLH-1 in *clh-1* knockout under the same promoter fails to rescue (Fig. 1B). Furthermore, knockdown of *twk-33*, another unrelated AMsh glia expressed gene, using the T02B11.3 promoter does not cause nose touch insensitivity (Fig. 1B). These data support a glial-specific function for CLH-1 in nose touch avoidance behavior. Finally, for comparison, we assayed nose touch avoidance response of nose touch insensitive *deg-1(u38u421)* and *trpa-1(ok999)* mutants and obtained similar results. DEG-1 and TRPA-1 are mechanosensitive channels expressed in ASH, and ASH and OLQ neurons, respectively (Hart et al., 1999, Kindt et al., 2007). Taken together, these data support that CLH-1 is needed in AMsh glia for nose touch responses.

AMsh glia influence the development of sensory cilia in *C. elegans* (Heiman and Shaham, 2009) and the *Drosophila* homologous chloride channel ClC-a, expressed in glial stem cell niche, participates in neurogenesis (Plazaola-Sasieta et al., 2019). Thus, the nose touch insensitive phenotype of *clh-1* worms could be caused by defective development of ASH sensory cilia. To check for this possibility, we imaged GFP labeled ASH neurons in *clh-1* knockout worms (Fig. 1E). We found no abnormalities, in particular the length and the area of the cilia were just like those of wild type animals (Fig. 1F and G, respectively). Collectively, these results support that Cl^- channel CLH-1 is needed in AMsh glia for the function of the nose touch sensing neurons ASH, rather than for their structure.

CLH-1 is needed in glia for ASH touch adaptation.

To discern how glial CLH-1 influences nose touch behavior, we analyzed *in vivo* ASH neurons' responses to two consecutive mechanical stimulations using the genetically encoded Ca^{2+} sensor GCaMP-6s. First, in wild type animals, similarly to what has been seen in ASH neurons upon exposure to aversive odors (Duan et al., 2020), the Ca^{2+} transient elicited by the second touch is smaller than that elicited by the first touch (Fig. 2A, left and middle panels). Interestingly, smaller Ca^{2+} transients also decay faster, suggesting faster Ca^{2+} removal/buffering when Ca^{2+} rises to lower concentrations (Fig. 2A, right panel). In *clh-1* mutants though, this adaptation is not present and the Ca^{2+} transients elicited by the two consecutive touches are similar in amplitude and decay time (Fig. 2B). Importantly, similar results were obtained using a smaller force (30 μN instead of 87 μN), (Fig. S1D and E), suggesting that *clh-1* knockout does not change ASH neurons' sensitivity to force (Geffeney et al., 2011). Consistent with the nose touch behavioral assays (Fig. 1B), expression of CLH-1 in ASH did not restore the Ca^{2+} transients' wild type phenotype (Fig. 2C). On the other hand, expression of CLH-1 in AMsh glia did. Indeed, adaptation and faster decay of the Ca^{2+} transients are both fully restored in these transgenic animals (Fig. 2D).

Consistent with a previous publications showing that DEG-1 is a mechanosensitive channel in ASH (Geffeney et al., 2011), *deg-1* mutants responded to touch stimulation with very small Ca^{2+} transients (Fig. 2E). As shown in Fig. 1B, *trpa-1* mutants are also nose touch insensitive, however, as reported by Kindt and colleagues, TRPA-1 functions in both ASH and OLQ nose touch neurons. Thus, the combined lack of this channel in both neurons produces the nose touch insensitive phenotype (Kindt et al., 2007). Not surprisingly, and similar to Kindt and colleagues, we still detected Ca^{2+} transients in *trpa-1* mutants, albeit of slightly smaller amplitude as compared to wild type (10.6 ± 3.6% vs 15.1 ± 2.5% of wild type, $p = 0.9982$, Fig. 2F left panel). Adaptation and Ca^{2+} transients' decays in *trpa-1* mutants were similar to *clh-1* knockout animals, although a trend to adaptation persisted (Fig. 2F middle and right panels).

Our data so far show that *clh-1* knockout worms are nose touch insensitive (Fig. 1B) and that they also display loss of adaptation of ASH Ca^{2+} transients (Fig. 2B). These results are surprising but suggest that cellular adaptation is required for nose touch sensitivity, and that behavioral adaptation might not be linearly related to ASH adaptation. To further investigate this idea, we analyzed the behavioral response to consecutive touches in wild type, *clh-1*, and *clh-1* rescue strains, and in the nose touch insensitive controls *deg-1* and *trpa-1* mutants. We found no statistical difference between the first two touches (Fig. S2). However, we noticed some adaptation across five touches in the wild type and AMsh glia rescue strains (Fig. S2A and E). Although, by comparing cellular and behavioral adaptation, we found that they had different decays. While 56% of decay is seen in wild type ASH Ca^{2+} transients upon 2 touch stimulations (Fig. 2A), similar decay would require ~15 touches in behavioral experiments (Fig. S2A). To further investigate this, we repeated the behavioral experiments in wild type waiting 2 minutes, like we do for imaging experiments, instead of 30 seconds, between touches. We found no adaptation at all under these conditions (Fig. S2G and J). These results are distinct from what has been recently reported by Duan and colleagues, who showed that ASH adaptation corresponds to behavioral adaptation to isoamyl alcohol and octanol (Duan et al., 2020). Interestingly, *clh-1* mutants show normal adaptation to octanol (Fig. S1F), in addition to responding to this odor just like wild type (Fig. 1D). This result supports that CLH-1 is specifically needed for nose touch avoidance behavior. To allow further comparison between behavioral and Ca^{2+} imaging, we performed behavioral assays on wild type and *clh-1* using a glass probe similar to that used in Ca^{2+} imaging, instead of an eyelash which is normally used in behavioral assays, and we obtained similar results (Fig. S2H-I and K). We conclude that CLH-1 mediates ASH neurons' adaptation to consecutive touches and that loss of adaptation correlates with behavioral nose touch insensitivity (Table S1).

The response to touch of AMsh glia.

Isoamyl alcohol and octanol are sensed by AMsh glia via glial-specific G-protein coupled receptors and AMsh glia have been shown to respond to nose touch by activation of depolarizing currents and Ca^{2+} transients (Ding et al., 2015, Duan et al., 2020). Therefore, we wondered whether glial *clh-1* regulated AMsh glia responses to nose touch stimulation. Consistent with a previous publication (Ding et al., 2015), we observed Ca^{2+} transients in AMsh glia upon nose touch stimulation. These transients were slower than those seen in ASH neurons and adapted more robustly. Indeed, virtually no Ca^{2+} transients were seen upon stimulation with the second touch (Fig. 3A). More importantly though, we observed the same phenotype in *clh-1* knockout animals (Fig. 3B). Ca^{2+} transients and decay times were not statistically different between wild type and *clh-1* knockout. These results show that glial Cl^- channel CLH-1 is not needed for AMsh glia Ca^{2+} response to nose touch.

Being that CLH-1 is a Cl^- channel, we next wondered whether CLH-1 influenced Cl^- concentration in AMsh glia. We thus analyzed *in vivo* Cl^- changes in AMsh glia upon two consecutive touches in animals expressing the chloride sensor SuperClomeleon under the control of the AMsh glia promoter T02B11.3 (Park et al., 2021). In wild type, we found that while intracellular Cl^- rises upon the first touch stimulation (Fig. 3C, left panel and E), it decreases upon the second touch stimulation (Fig. 3C, right panel and E). Interestingly, these changes in intracellular Cl^- concentration are slow and do not return to control level (pre-touch stimulation) during the course of the 120 seconds recording, long after the touch stimulation has ceased. In *clh-1* knockout, there is also an increase of intracellular Cl^- upon first touch stimulation that has the same kinetics and amplitude of the one observed in wild type animals, ruling out that it is mediated by CLH-1 (Fig. 3D, left panel and E). Moreover, *clh-1* knockout has a basal intracellular Cl^- concentration in AMsh glia similar to that of wild type (YFP/CFP baseline ratios: 1.38 and 1.42 for wild type and *clh-1* respectively, not statistically different). However, the Cl^- decrease observed in wild type animals upon second touch stimulation, is completely absent in *clh-1* (Fig. 3D, right panel and E). These results are consistent with Cl^- influx in AMsh glia upon first touch stimulation being mediated by a channel or transporter other than CLH-1. This channel/transporter could be directly gated by mechanical forces or could be activated indirectly by rise of intracellular Ca^{2+}. But more importantly, our results support that there is Cl^- efflux from AMsh glia following stimulation with the second touch and that this is mediated by CLH-1. This is consistent with the fact that CLH-1 is an inward rectifier Cl^- channel and thus conducts Cl^- ions preferably in the outward direction (Grant et al., 2015). To conclude, AMsh glia undergo changes in Ca^{2+} and Cl^- concentrations during touch stimulation and Cl^- channel CLH-1 is responsible for Cl^- efflux during stimulation by second touch.

GABA signaling mediates ASH adaptation to consecutive touches.

Adaptation of ASH neurons following consecutive exposures to aversive odors is mediated by glial GABA through the activation of $GABA_A$ receptors LGC-38 expressed in ASH neurons (Duan et al., 2020). To test whether ASH adaptation to mechanical stimulation is mediated by the same mechanism, we used pharmacological and genetic approaches. We found that ASH adaptation is absent in wild-type animals treated with the $GABA_A$ antagonist bicuculline (Fig. 4A, left and middle panels) (Duan et al., 2020). To further confirm the involvement of GABA signaling, we performed ASH Ca^{2+} imaging experiments in mutants of the GABA synthesis enzyme *unc-25* and in animals in which *unc-25* was knocked down in AMsh glia. We found that also in these cases ASH adaptation to two consecutive touches was absent (Fig. 4B and C, left and middle panels). Finally, to establish whether ASH adaptation is mediated cell-autonomously by LGC-38 receptors, we performed experiments in worms in which *lgc-38* was knocked down in ASH neurons. Again, ASH neurons adaptation was not present (Fig. 4D, left and middle panels). The lack of ASH adaptation in these experimental conditions and strains was associated with similar decay time of the Ca^{2+} transients upon stimulation with the two touches (Fig. 4A-D, right panels), similarly to what seen in *clh-1* mutants. We showed that expression of CLH-1 in AMsh glia rescues nose touch avoidance and Ca^{2+} transients' adaptation (Fig. 1B and 2D). To determine whether this rescue is mediated by GABA signaling, we performed experiments in CLH-1 rescue strain in the presence of bicuculline. We found loss of rescue (Fig 4E).

At the behavioral level, animals treated with bicuculline, mutant or AMsh glia-knocked-down for *unc-25*, and with ASH specific knockdown of *lgc-38*, were all nose touch insensitive (Fig. 4E). These results again underscore that lack of ASH adaptation to touch correlates with nose touch insensitivity (Table S1) and demonstrate that GABA signaling is required for behavioral responses to nose touch. These animals also responded similarly to the first two touches (no statistical difference) and no adaptation was observed upon 5 touches (Fig. S3A-F). We conclude that ASH adaptation to consecutive touches is mediated by GABA signaling.

Chloride ions are needed for ASH adaptation and for behavioral responses to nose touch.

We found that CLH-1 is needed for Cl^- efflux from AMsh glia following stimulation by second touch (Fig.3C-E). Since $GABA_A$ receptors are Cl^- channels, we hypothesized that the function of CLH-1 might be to provide Cl^- ions needed for GABA signaling to the extracellular environment surrounding ASH. Thus, we predicted that supplementing *clh-1* knockout worms with more Cl^- could rescue nose touch insensitivity and ASH adaptation to touch. We reared *clh-1* knockout worms on plates enriched with NaCl or KCl (Johnson et al., 2020, Singhvi et al., 2016) and assayed nose touch avoidance behavior and ASH Ca^{2+} transients. We found that *clh-1* worms grown in Cl^- enriched plates, showed a significant rescue of the nose touch insensitive behavioral phenotype (Fig. 5A), while the nose touch phenotype of wild type, *deg-1*, and *trpa-1* mutants was not affected by these conditions. To eliminate the possibility that this effect is caused by increased osmolarity of the NaCl and KCl enriched plates, we used sucrose, Na-acetate, and Na-gluconate enriched plates as a control. We found that *clh-1* knockout worms reared on these plates remained nose touch insensitive (Fig. 5A). We conclude that the nose touch insensitive phenotype of *clh-1* knockout worms is significantly rescued by increased levels of Cl^-. These results support the idea that CLH-1 in AMsh glia provides the extracellular Cl^- ions needed for GABA inhibition of ASH neurons, as suggested by the Cl^- imaging data shown in Fig. 3 C-E, thus corroborating that CLH-1 and GABA signaling are part of the same pathway. To further test this, we performed nose touch experiments in *clh-1* knockout animals in which we knocked down *unc-25* in AMsh glia and in *clh-1* knockout in which we knocked down *lgc-38* in ASH. We found that both these strains were as nose touch insensitive as *clh-1* knockout, supporting that these genes belong to the same pathway (Fig. 4E).

We next looked at ASH Ca^{2+} transients in wild type and *clh-1* worms grown on KCl enriched plates. We found that while ASH adaptation in wild type worms was for the most part unaffected, adaptation was restored in *clh-1* knockout worms (Fig. 5B and C). Interestingly, the time of decay of the Ca^{2+} transients upon the second touch stimulation was similar to the first touch in both strains. We attribute this to the larger Ca^{2+} transients in ASH neurons of wild type animals reared in KCl enriched plates and to the significant rescue conferred by KCl in *clh-1* mutants (Fig. 5B and C, right panels). Also in this case, some adaptation was seen across 5 touches in wild type and *clh-1* reared on KCl plates, although there was no statistical difference between the first two touches (Fig. S4A-D)(Duan et al., 2020). Taken together, the Ca^{2+} imaging data support that Cl^- ions, in addition to being needed for behavioral response to touch, are also needed for ASH cellular adaptation. To establish whether Cl^- ions are needed for GABA signaling, we repeated the experiments on wild type and *clh-1* worms reared on KCl plates in the presence of bicuculline or following knock-down of *lgc-38* in ASH. We found loss of rescue in ASH Ca^{2+} transients' adaptation and behavior, confirming that supplemented Cl^- ions are needed for GABA signaling (Fig. 5D-G and Fig. S4E-J).

The *clh-1* homolog *clh-3* is also enriched in AMsh glia (Grant et al., 2015). This channel, just like CLH-1, is an inward rectifier (Rutledge et al., 2001). We thus wondered if *clh-3* was also needed for nose touch responses. We found that *clh-3* knockout animals respond normally to nose touch and that knockout of this gene does not worsen the *clh-1* nose touch insensitive phenotype (36.67% ± 0.044 vs 30.76% ± 0.013 in *clh-1*, Fig. 5H and Fig. S5A-B). These data indicate that *clh-3* is not required for nose touch responses in *C. elegans*. However, we found significant rescue of the *clh-1* nose touch insensitive phenotype in animals overexpressing CLH-3 in AMsh glia (Fig. 5H and Fig. S5C). These results again support the need of a Cl^- channel in AMsh glia for flux of Cl^- probably in the microenvironment between glia and ASH neurons. Interestingly though, knockout of *kcc-3*, an AMsh glial K^+/Cl^- cotransporter that regulates the structure and function of thermosensory neurons AFD, has no effect on nose touch avoidance (Fig. 5H). This result is in line with the very restricted localization of KCC-3 in AMsh glial membrane's microdomains facing AFDs cilia, as reported by Singhvi and colleagues (Singhvi et al., 2016).

Is the function of CLH-1 conserved across species? Mammalian ClC-2 is expressed in oligodendrocytes and astrocytes where it controls Cl^- efflux (Hou et al., 2018, Sik et al., 2000). The exact role of ClC-2 in mammalian glia is still poorly understood but mutations in ClC-2 cause epilepsy and leukoencephalopathy in humans and mice, a brain disorder characterized by vacuolation of the white matter (Blanz et al., 2007, Depienne et al., 2013, Saint-Martin et al., 2009). To test whether ClC-2 could complement for the lack of CLH-1 in AMsh glia, we tested nose touch responses in *clh-1* mutants expressing rat ClC-2 in AMsh glia and observed a rescue in phenotype (Fig. 5H and Fig. S5D). Growth in KCl enriched plates slightly ameliorated nose touch responses, but results were not statistically different (Fig. 5H and Fig. S5E). Thus, these results support that CLH-1 and ClC-2 are functional homologs.

CLH-1 is also bicarbonate (HCO_3^-) permeable and plays a role in pH regulation (Grant et al., 2015). Coincidentally, $GABA_A$ receptors permeate both HCO_3^- and Cl^- with a HCO_3^-/Cl^- of 0.2-0.4 (Ma et al., 2012). Thus, in the absence of Cl^- and at high concentration of extracellular bicarbonate, LGC-38 could lead to ASH hyperpolarization by permeating HCO_3^-. To determine the role of bicarbonate, we assayed nose touch responses in worms that were grown in plates supplemented with $KHCO_3$ or with KCl + $KHCO_3$ (Fig. S6A-I). We found that *clh-1* worms grown in $KHCO_3$ and KCl + $KHCO_3$ supplemented plates showed significant rescue of nose touch sensitivity (Fig. S6A and D). However, in worms expressing rat ClC-2 in AMsh glia, $KHCO_3$ supplementation partially suppressed rescue (Fig. S6A and E). This effect might be due to inhibition of highly pH sensitive ClC-2 by the more alkaline pH caused by $KHCO_3$ supplementation (Arreola et al., 2002). This conclusion is supported by the fact that the negative effect of $KHCO_3$ disappears in animals reared in KCl + $KHCO_3$ supplemented plates. To conclude, while we cannot exclude long term effects of the plate supplementations, our data support that Cl^- or HCO_3^- flux in glia is required for nose touch avoidance response and ASH adaptation to touch.

Glial CLH-1 and cAMP signaling.

As mentioned above, Duan and colleagues found that upon multiple exposures to the aversive odors isoamyl alcohol and octanol, both ASH Ca^{2+} transients and animal behavior adapt via GABA signaling (Duan et al., 2020). Similarly, we find that GABA signaling mediates ASH cellular adaptation to touch. However, at the behavioral level, GABA signaling is required for nose touch avoidance even upon the first touch stimulation (Fig. 4). This suggests that ASH hyperpolarization mediated by GABA is required for a cellular signaling cascade that eventually leads to nose touch avoidance behavior.

Aversive responses to quinine and serotonin in *C. elegans* are mediated by the co-release of glutamate and neuropeptides (Harris et al., 2010). In these conditions, the release of neuropeptides such as NLP-3 is mediated by the cGMP and cAMP signaling (Harris et al., 2010, Krzyzanowski et al., 2016). We thus hypothesized that CLH-1 (and GABA) might be needed for cyclic nucleotides signaling. If this hypothesis is correct, then in the absence of *clh-1*, nose touch avoidance behavior might be rescued by inhibition of cyclic nucleotide degradation. We thus performed nose touch assays in phosphodiesterase mutants in which we knocked down *clh-1* in AMsh glia (Fig. 6A and Fig. S7). We found that, while quadruple mutant of cGMP phosphodiesterase genes *pde-1; pde-5; pde-3; pde-2* did not rescue the nose touch insensitivity of *clh-1* AMsh glia RNAi, knockout of cAMP specific phosphodiesterase *pde-4* did. This result was confirmed in *clh-1; pde-4* double mutant animals (Fig. 6A and Fig S7A-E). Interestingly, *pde-4* knockout rescues also *deg-1* mutant nose touch insensitivity (Fig 6A and Fig. S7F). This result places cAMP signaling downstream of DEG-1 channels. To further test the role of cAMP in nose touch avoidance, we overexpressed *pde-4* in ASH neurons using the *sra-6* promoter. We found that these transgenic animals, that are expected to have low levels of cAMP in ASH neurons, are nose touch insensitive (Fig. 6A and Fig. S7G). This phenotype is rescued by cultivation on Cl^- enriched plates suggesting that ASH membrane hyperpolarization might elevate cAMP levels in these transgenic animals possibly via activation of ACY-1 (Fig. 6A and Fig. S7H).

We next tested our hypothesis by both pharmacological and genetic hyperactivation of adenylyl cyclase. We found that *clh-1* mutants treated with the adenylyl cyclase activator forskolin showed significant rescue of their nose touch insensitive phenotype (Fig. 6B and Fig. S8A-C). Similarly, *clh-1* mutants expressing a hyperactive adenylyl cyclase *acy-1* (*acy-1(md1756)*) showed rescue of the nose touch insensitive phenotype (Fig. 6C and Fig. S8D-E). Again, *deg-1* mutant phenotype was significantly rescued by genetic hyperactivation of adenylyl cyclase, underscoring once again that cAMP signaling is downstream of DEG-1 channel (Fig. 6C and Fig. S8F). In addition, in support of our hypothesis, we found that *nlp-3* knockout mutants and animals in which *nlp-3* has been knocked down using the *sra-6* promoter are nose touch insensitive, establishing that this peptide is needed in ASH neurons for nose touch avoidance behavior (Fig. 6D and Fig. S8G-H).

How might Ca^{2+} and cAMP signaling cooperate in ASH neurons to drive nose touch avoidance behavior? Our results and previous studies suggest a possible mechanism (Fig. S9). Elevation in intracellular Ca^{2+}, caused by activation of DEG-1, and possibly another mechanosensitive channel, causes glutamate release from ASH neurons (Piggott et al., 2011). At the same time, cAMP signaling is needed for the release of the peptide NLP-3 from ASH (Fig. 6D)(Harris et al., 2010). While NLP-3 unequivocally leads to avoidance response via activation of interneurons AVA and AIB (Harris et al., 2010), glutamate can suppress nose touch avoidance if released at high levels via activation of lower affinity receptor GLR-5 expressed in AIB neurons (Zou et al., 2018). Indeed, GLR-5 in AIB has been shown to promote the activity of inhibitory interneuron RIM (Zou et al., 2018). To directly test this model, we first knocked down the vesicular glutamate transporter *eat-4* in ASH of *clh-1* knockout animals and we overexpressed it in wild type animals. As predicted by the model (Fig. S9), we found that while reducing glutamate release significantly rescued nose touch avoidance in *clh-1*, increasing glutamate release in wild type animals caused significant loss of nose touch sensitivity (Fig. 6D and Fig. S8I-J). Second, to further test this model, we knocked down *glr-5* in AIB of *clh-1* knockout animals. As expected, we found significant rescue of nose touch avoidance in these animals (Fig. 6D and Fig. S8K).

The nose touch insensitivity of *clh-1* knockout upon first touch stimulation might be explained by elevated basal Ca^{2+} concentration in this mutant as opposed to wild type. To test this hypothesis, we quantified the basal GCaMP-6s fluorescence in ASH neurons. We found that *clh-1* knockout animals have higher fluorescence as compared to wild type, indicative of higher basal Ca^{2+} in these mutants (Fig. 6E). Similarly, nose touch insensitive bicuculline-treated wild type animals have higher fluorescence than nose touch sensitive *clh-1* and wild type reared on Cl^- enriched plates (Fig. 6E). Thus, we conclude that to prevent high levels of glutamate release from ASH, which would cause reduced nose touch avoidance response upon consecutive touch stimulations, GABA signaling via AMsh glia is engaged, resulting in control of the level of Ca^{2+} in ASH neurons. But our data overall reveal something else: CLH-1 and GABA signaling keep the basal concentration of Ca^{2+} in ASH neurons low. This suggests that there is tonic GABA release from AMsh glia, a phenomenon that has been described in other systems (Lee et al., 2010, Kwak et al., 2020).

To determine the role of cAMP signaling in the control of intracellular Ca^{2+} in ASH neurons upon touch stimulation, we performed imaging experiments. Strikingly, we found that both knockout of *pde-4* and hyperactivation of *acy-1* rescued adaptation and faster Ca^{2+} transients upon second touch stimulation of *clh-1* mutants (Fig. 7A-D). These results support two important conclusions: 1) cAMP is important for ASH adaptation, suggesting that cAMP plays a role in Ca^{2+} homeostasis and 2) the role of glial chloride is upstream of cAMP. We conclude that the Cl^- channel CLH-1 is needed in AMsh glia for regulation of Ca^{2+} levels and indirectly influences the cAMP pathway in ASH mechanosensory neurons. Thus, our data support that glial CLH-1 is a key regulator of the activity of mechanosensory neurons ASH.

DISCUSSION

In this work we report for the first time that a Cl^- channel of the ClC family is needed in glia to regulate responses to touch stimulation. More specifically, we show that the glial Cl^- channel CLH-1 is needed for GABA regulation of excitability and for regulation of cAMP levels in a mechanosensory neuron in *C. elegans*. Our work also demonstrates for the first time that two parallel and interconnected intracellular messengers' pathways involving Ca^{2+} and cAMP work together in polymodal ASH neurons to drive nose touch avoidance behavior (Fig. 8). Our data support an exquisite cooperation between mechanosensory neurons and associated glia in mediating the animal's sensitivity to touch. Given the fact that components of the GABA and cAMP signaling pathways have been reported in touch receptors and nociceptors in mammals (Celotto et al., 2019, Pawson et al., 2009, Zhu et al., 2014), and that CLH-1 mammalian homolog ClC-2 is expressed in glia and other accessory cells (Blanz et al., 2007, Depienne et al., 2013), we propose that the mechanism we have uncovered is conserved across species.

Nose touch responses in *C. elegans* are initiated by the activation of mechanosensitive DEG/ENaC channel DEG-1 in polymodal ASH neurons (Geffeney et al., 2011), although other mechanosensitive neurons participate (Kindt et al., 2007). Activation of DEG-1 causes membrane depolarization which in turn is expected to activate voltage-gated calcium channels (VGCC). The VGCC EGL-19 is the most likely candidate, as it has been shown to mediate elevation of intracellular Ca^{2+} in body touch neurons, ASH neurons, and other sensory neurons upon stimulation (Kato et al., 2014, Suzuki et al., 2003). However, we found that upon stimulation with a second touch, increase of intracellular Ca^{2+} was dampened (Fig. 2A). Contrary to what is seen for responses to octanol and isoamyl alcohol (Duan et al., 2020), the reduced Ca^{2+} transients upon the second nose touch stimulation do not correlate with behavioral adaptation. On the contrary, comparison of the Ca^{2+} imaging and behavioral data strongly supports that the ASH Ca^{2+} adaptation is required for nose touch sensitivity. Mutations and pharmacological treatments that eliminate ASH Ca^{2+} adaptation correlate with nose touch insensitivity (Fig. 4 and Table S1). Importantly, nose touch insensitivity in *clh-1* knockouts is also seen upon stimulation with the first touch

(Fig. S2D). Our model predicts that this could be caused by elevated intracellular Ca^{2+} at baseline (Fig. S9). Indeed, as shown in Fig. 6E, intracellular Ca^{2+} at baseline is higher in nose touch insensitive *clh-1* as compared to nose touch sensitive wild type, and wild type and *clh-1* reared on Cl^- enriched plates. Higher Ca^{2+} levels at baseline are also observed in wild type animals treated with bicuculline, suggesting tonic GABA release from AMsh glia under normal conditions.

As shown for octanol and isoamyl alcohol (Duan et al., 2020), ASH cellular adaptation to touch is mediated by AMsh glial GABA via activation of $GABA_A$ receptor LGC-38 expressed in ASH neurons. The only location in which AMsh glia and ASH are in close proximity is at the sensory neuronal endings, where the AMsh glia ensheath the ASH dendrites. While we cannot exclude that GABA released from AMsh glia diffuse long distances to act on other ASH subcellular locations, *C. elegans* anatomy support that GABA signaling is from AMsh glial endings to the ASH dendritic endings (the cilia). Thus, taken together our data support the idea that tonic and phasic GABA signaling in nose touch receptors is required for responses to touch (Farrant and Nusser, 2005). This is an intriguing finding because GABA signaling has been described in at least one vertebrate touch receptor, the Pacinian corpuscle (Pawson et al., 2009). Immunochemical, electrophysiological, and pharmacological studies have shown that $GABA_A$ receptors are expressed on the nerve ending of the Pacinian corpuscle of the cat and that block of these receptors by gabazine or picrotoxin increases action potential firing during the static portion of a sustained indentation stimulus (Pawson et al., 2009). These studies thus concluded that GABA is required for the rapid adaptation of the Pacinian corpuscles, a mechanism that is thought to be essential for detecting vibrations. Our data support that the Cl^- channel of the ClC family expressed in glia associated with mechanosensors provide the Cl^- ions that are needed for GABA signaling (Fig. 3C-E and Fig. 4). It will be important to establish whether a Cl^- conductance is present in the inner lamellae of the Pacinian corpuscle and whether this is needed for the function of these touch receptors.

Importantly, ClC-2, the mammalian homolog of CLH-1, is expressed in astrocytes and oligodendrocytes (Hou et al., 2018, Sik et al., 2000) and a role of ClC-2 in controlling extracellular Cl^- concentration has been suggested based on the phenotype caused by mutations in this channel. Indeed, mutations in ClC-2 cause vacuolization of the white matter in both humans and mouse models (Blanz et al., 2007, Depienne et al., 2013). Similarly, loss of ClC-2 in the Sertoli cells and the pigmented epithelium of the eye causes the degeneration of spermatocytes and photoreceptors, respectively, probably due to dysregulation of Cl^- homeostasis (Bosl et al., 2001). Finally, a new variant of ClC-2 has been associated with the genetic etiology of Tourette syndrome, which is characterized by chronic tics and reduced adaptation to tactile stimulation (Yuan et al., 2020). Intriguingly, Tourette syndrome patients have reduced GABA signaling in the sensorimotor cortex (Puts et al., 2015), but it might be interesting to determine whether there are also defects in GABA signaling at the level of the peripheral mechanosensors.

AMsh glia respond to mechanical stimulation with Ca^{2+} transients (Fig. 3A-B) (Ding et al., 2015). Contrary to what seen with octanol and isoamyl alcohol though, AMsh glia adaptation to the second touch stimulation is almost complete (Fig. 3A-B). This phenomenon argues against GABA vesicular release from AMsh glia since the ASH adaptation by GABA becomes evident on the second touch (Fig. 4). One possible mechanism of GABA release is via bestrophin channels (Kwak et al., 2020). Future studies will establish which one of the 26 members of this family might be mediating GABA release from AMsh glia.

Our experiments also reveal a prominent role for cAMP signaling in nose touch responses and ASH Ca^{2+} transients' adaptation. Indeed, nose touch defects caused by loss of CLH-1 in glia are rescued by genetic and pharmacological interventions that elevate intracellular cAMP levels (Figs. 6A-C, S7 and S8A-F). Furthermore, these interventions rescue ASH Ca^{2+} transients' adaptation (Fig. 7). It is not clear how ASH neurons achieve this compensation, but one possibility is via PKA phosphorylation of downstream effectors, such as K^+ channels or the Na^+/Ca^{2+} exchanger, that might help hyperpolarize the membrane of ASH neurons and/or remove intracellular Ca^{2+} (Fig. 8). In wild-type animals, glial CLH-1 might regulate the function of adenylyl cyclase either via Cl^-, similarly to how AMsh glial-expressed KCC-3 regulates the function of guanylyl cyclase GCY-8 in AFD neurons (Singhvi et al., 2016), though in this case the regulation would be via intracellular rather than extracellular Cl^- (Figs. 4E, 5D-G, S4E-J) or indirectly via regulation of intracellular Ca^{2+} (Fig. 8). Intriguingly, worm ACY-1 shares 40% identity with mammalian ADCY3, which is inhibited by Ca^{2+} via Ca^{2+}/calmodulin kinase phosphorylation at a serine that is conserved in ACY-1 (Halls and Cooper, 2011, Wei et al., 1998). While our data support a model in which cAMP and Ca^{2+} signaling in ASH work together to mediate nose touch avoidance behavior, the strong Ca^{2+} transients adaptation seen in ASH upon second touch stimulation suggests that the function of other touch neurons, potentially influenced by CLH-1, may also be recruited (Kindt et al., 2007).

The fact that elevation of cAMP rescues also *deg-1* loss-of-function mutants suggests that cAMP is downstream of DEG-1 and that another mechanosensitive channel must be present in ASH neurons, as suggested by our Ca^{2+} imaging results and by Geffeney and colleagues (Fig. 2E) (Geffeney et al., 2011). This channel may also induce cAMP signaling or its function might be potentiated either directly or indirectly via cAMP signaling. The discovery of cAMP signaling in nose touch responses in *C. elegans* is particularly exciting because in mammals, enhanced cAMP/PKA signaling has been shown to cause hyperexcitability of sensory neurons and has been linked to mechanical hyperalgesia and allodynia (Lolignier et al., 2015). Thus, studying ASH signaling and how it is modulated by glia could help to shed new light onto mechanisms of chronic pain. To conclude, our data support that glial Cl^- CLH-1 is needed for GABA signaling, and directly or indirectly to regulate Ca^{2+} and cAMP levels in ASH neurons. Thus, collectively our results support the idea that CLH-1 is a key regulator of nose touch avoidance.

STAR METHODS

RESOURCE AVAILABILITY

Lead contact—Further information and requests for resources should be directed to and will be fulfilled by the lead contact, Laura Bianchi (l.bianchi@med.miami.edu)

Materials Availability—DNA constructs and *C. elegans* strains generated in this study are available upon request.

Data and Code Availability—All data reported in this paper will be shared by the lead contact upon reasonable request.

This paper does not report original code.

Any additional information required to reanalyze the data reported in this paper is available from the lead contact upon request.

EXEPERIMENTAL MODEL AND SUBJECT DETAILS

All nematode strains were maintained under standard conditions, at 20°C on nematode growth medium (NGM) seeded with *Escherichia coli* (OP50 strain) as previously described (Brenner, 1974). The Bristol N2 strain was used as wild type control. All worms used in this study were healthy and well-fed day 1 (D1) young adult hermaphrodites. All worms were drug or test naïve prior to supplementation or pharmacological treatment (see Methods Details for further information about plates supplementation and drug treatments). A full list of strains and genotypes used in this study is provided in the Key Resources Table. Strains BLC315, BLC328, BLC371, BLC401, BLC402, BLC441, BLC447, BLC448, BLC449, BLC453, BLC455, BLC456, BLC338, BLC496, BLC497, BLC498, BLC500, BLC501, BLC502, BLC503, BLC504, BLC505, and BLC506 were obtained by injecting the corresponding DNA constructs as previously described (Mello et al., 1991). Strain BLC454 was obtained by crossing strains BLC401 and RB833. Strain BLC469 was obtained by crossing strains BLC402 and RB833. Strain BLC375 was obtained by picking not fluorescent worms from the previously reported strain BLC297 (Grant et al., 2015). BLC450 was obtained by crossing strains KG744 and BLC454. BLC444 was obtained by crossing strains KG744 and TU38. BLC451 was obtained by crossing strains BLC454 and KG522. BLC435 was obtained by crossing strains KG521 and TU38. BLC457 and BLC458 were obtaining by crossing KG744 and KG522, respectively, with BLC454 and selecting worms expressing the fluorescent reporters and genotyped to *clh-1* wild type alleles. BLC499 and BLC407 were obtained by crossing BLC498 and BLC500, respectively, with RB833.

METHOD DETAILS

Molecular biology

Plasmid construction for rescue or overexpression.: Plasmids generated for *C. elegans* injection were created using the vector pPD95_75, a gift from Andrew Fire (Addgene plasmid # 1494; http://n2t.net/addgene:1494 ; RRID:Addgene_1494). To label ASH neurons with RFP, we constructed *pSra-6::RFP* by replacing *delm-1* with *RFP* from the previously reported *pSra-6::delm-1* and $P_{delm\text{-}1}$*::RFP* constructs (Han et al., 2013), respectively. To rescue CLH-1 expression in ASH neurons, we built the *pSra-6::clh-1 (cDNA)* construct by replacing *delm-1* for *clh-1* (cDNA) from the previously described constructs *pSra-6::delm-1* (Han et al., 2013) and *pGEM+clh-1 cDNA* (Grant et al., 2015), respectively. To image calcium transients in ASH neurons and in AMsh glia, *pSra-6::GcaMP-6s* and *pT02B11.3::GcaMP-6s* were made by replacing *clh-1* (cDNA) from the *pSra-6::clh-1* *(cDNA)* or *pT02B11.3::clh-1 (cDNA)* constructs of this study, respectively, with *GcaMP-6s* from the plasmid *pPD_Pnpr-4::G-CaMP6s*, a gift from Shohei Mitani (Addgene plasmid # 117423; http://n2t.net/addgene:117423 ; RRID:Addgene_117423)(Hori et al., 2018). To build the amphid sheath glia rescue constructs, *clh-1* cDNA from *pGEM+clh-1 cDNA* (Grant et al., 2015), *clh-3b* cDNA from *pENTR221+clh-3b cDNA*, a gift from William R. Schafer (Branicky et al., 2014), and rat *ClC* cDNA from *pTLN+rClC-2 cDNA*, a gift from Michael Push, were independently cloned into the *pPD95.75* vector containing the amphid sheath glia promoter *pT02B11.3* (Bacaj et al., 2008). To build the Amsh glia rescue using the *vap-1* promoter, *clh-1* cDNA from *pT02B11.3::clh-1* construct was used to replace *RFP* gene in the *Pvap-1::RFP* plasmid (Johnson et al., 2020). To image endogenous CLH-1 expression in amphid sheath glia, *pT02B11.3::GFP1-10* DNA was made by replacing *clh-1* cDNA from *pPD95_75 (pT02B11.3::clh-1 cDNA)* with *GFP1-10* from the *pSH87(Pflp-13::gfp1-10)* construct, a gift from David M. Miller (Addgene plasmid # 127705 ; http://n2t.net/addgene:127705 ; RRID:Addgene_127705)(He et al., 2019). To image Cl^- in Amsh glia, we replaced *clh-1* with codon optimized SuperClomeleon, a gift from Hirofumi Kunitomo (Park et al., 2021), in the *pT02B11.3::clh-1 (cDNA)* construct. To overexpress *pde-4* in ASH, we built the *Prsa-6::pde-4* construct by replacing GcaMP-6s with *pde-4* in the *Psra-6::GcaMP-6s* construct. The *pde-4* cDNA (isoform d) was from KG #203 (*Prab-3::pde-4d (+)* cDNA) and it was a gift from Kenneth Miller (Addgene plasmid # 110880 ; http://n2t.net/addgene:110880 ; RRID:Addgene_110880) (Charlie et al., 2006). To overexpress *eat-4* in ASH, we replaced *clh-1* with *eat-4* in the *Psra-6::clh-1* vector. The cDNA of *eat-4* (isoform a) was amplified by RT-PCR from mRNA and initially cloned into pCR2.1 – TOPO vector for amplification and sequence verification. One mutation resulting in a conserved amino acid substitution in a non-conserved domain was detected (733C>T resulting in amino acid change L245F) (Lee et al., 1999). Another mutation that did not result in amino acid change (747T>C (C249C)) was also found. The results observed using this *eat-4* sequence were as expected for the wild type sequence. These previously described constructs were also used: *pT02B11.3::pGM87* (Grant et al., 2015) and *Punc-122::GFP* as co-transformation markers.

RNA$_i$ constructs.: The Amsh glia specific knock-down of *clh-1, twk-33* and *unc-25*; the ASH specific knock-down of *clh-1, lgc-38, nlp-3 and eat-4;* and the AIB specific knock-down of *glr-5* were achieved following the methods previously described by Esposito and colleagues (Esposito et al., 2007). Briefly, a 407 bp fragment of the *clh-1* cDNA corresponding to exons 3 to 5, a 587 bp fragment of the *unc-25* cDNA from the *aptf-1p::unc25::sl2gfp* construct, a gift from Sreekanth H. Chalasani (Liu et al., 2018), corresponding to exons 1 to 5, a 752 bp fragment of the *lgc-38* genomic DNA corresponding to exons 7 to 10, a 314 bp fragment of the *nlp-3* genomic DNA corresponding to exons 1 to 2, a 591 bp fragment of the *eat-4* genomic DNA corresponding to exons 3 to 6, and a 722 bp fragment of the *glr-5* genomic DNA corresponding to exon 5 were amplified and fused with ~ 2 kb glial specific promoter pT02B11.3, ASH specific promoter *sra-6,* or AIB specific promoter *npr-9*, respectively, by PCR. To build the *twk-33* RNAi, sense and antisense fragments 396 bp from genomic DNA corresponding to exons 9 to 11 were independently cloned into the pPD95.75 vector under the control of the Amsh glia promoter T02B11.3.

Microscopy

Visualization of CLH-1 expression in AMsh glia.: The CRISPR-cas9 worms expressing CLH-1::GFP11, GFP1-10 in amphid sheath glia, and RFP in ASH neurons (BLC453 strain) were immobilized on 2% agarose (in M9 buffer) pads using 100 mM sodium azide. Fluorescent images were acquired using a Zeiss Axio Observer microscope equipped with an ORCA-Flash 4.0 V2 digital CMOS camera using a X63 water objective. The HCImage acquisition software was used to take the images, that were then processed with Fiji (ImageJ) software.

ASH morphology.: To determine the ASH cilium size, wild type or *clh-1* worms (CX3465 and BLC319, respectively) expressing GFP in ASH neurons were immobilized on 2% agarose (in M9 buffer) pads using 100 mM sodium azide. Images were taken with an Olympus IX81 confocal microscope equipped with an X60 oil immersion objective (Olympus) using a 488 nm laser (10% intensity). Image acquisition was performed with Olympus FluoView (Version 3.0a) at a scan speed of 8.0 μs per pixel and spatial resolution of 2028x2048 pixels, a 9.5 zoom over the cilia structure, and an average of ~ 6 “Z” stacks with 0.6 μm step size were acquired per sample. Images were then processed with Fiji (ImageJ software) using the “Z project” plugin with maximum intensity as projection type. Area and length of ASH cilia were quantified in the resulting projected images.

Calcium imaging.: To visualize the calcium transients in ASH neurons and in AMsh glia, worms expressing GCaMP-6s in ASH neurons or AMsh glia were glued (Gluture, FisherScientific, #NC0632797) onto 2% agarose pads prepared using extracellular saline solution (145 mM NaCl, 5 mM KCl, 1 mM $CaCl_2$, 5 mM $MgCl_2$, 20 mM D-glucose, 10 mM HEPES buffer, pH 7.2) and immersed in the same solution, as previously described (Kindt et al., 2007). Pads were then transferred to a 187 mm^3 chamber containing the same buffer. The chamber was mounted on an Olympus IX70 microscope with a X10 objective (Olympus) and a PCO SensiCam camera. The microscope was equipped with a Lambda DG-4 illumination system (Sutter Instrument Co.) as a light source and the excitation filter FF01-500/24-25 (Semrock) was used for strains expressing GCaMP-6s in ASH neurons and no other fluorophores. For strains ST2499 and ST2181, expressing RFP in AMsh glia and GCaMP-5 in ASH, the excitation filter FF01-488/10-25 (Semrock) was used to specifically excite GCaMP-5. The microscope was also equipped with a Lambda 10-2 optical filter changer to control emission before image acquisition. No emission filter was used for strains where there was no overlap with other fluorophores. The emission filter FF02-520/28-25 (Semrock) was used for strains ST2499 and ST2181 to capture only GCaMP-5 fluorescence. Images were acquired using MicroManager 2.0 software (Edelstein et al., 2014) at a frequency of 0.5 Hz with 100 ms exposure time and a spatial resolution of 1024x1024 pixels. ASH and AMsh glia recordings were 93 and 135 seconds long, respectively. For measuring basal calcium levels, the images corresponding to the 10 seconds before touch were stacked using the “Z project” tool with the maximum intensity projection type. The resulting image was then used to calculate pixel intensity. Only strains obtained by crossing with wild type expressing GCaMP-6s were used for this analysis. The pixel intensity values were normalized to wild type.

Touch stimulation in imaging experiments.: For nose touch stimulation, a borosilicate capillary glass (1.5 mm outer diameter, 0.86 mm inner diameter, Warner Instruments, # G150F-6) with the tip rounded with a fire polisher to ~10 μm was used. The probe was manipulated with a C-863 Mercury Servo Controller (Physik Instrumente) using the PIMikroMover software (version 2.4.4.6). The stimulation protocol consisted of placing the probe in a 45° angle close to the nose of the worm, retracting for 30 seconds, and then pushing it against the animal's nose providing a stimulation corresponding to 30 or 87 μN (Geffeney et al., 2011). The second touch stimulation was given 30 seconds after the first one. Images were then analyzed using Fiji (ImageJ) and plotted using GraphPad Prism (version 8.4.2). Data were normalized using the average fluorescence corresponding to the 10 seconds before touch stimulation. The decay time of each transient was calculated using the standard exponential fit tool from Clampfit software (version 10.7.0.3).

Chloride imaging.: For chloride imaging, the excitation filter FF02-438/24 (Semrock) was used to excite the sensor and the emission filters FF01-483/32 and FF01-542/27 were used to capture CFP and YFP fluorescence, respectively, for 120 seconds. SuperClomeleon is a YFP/CFP FRET-based chloride sensor in which YFP/CFP fluorescence ratio decreases upon binding to chloride ions (Park et al., 2021). For each frame, the fluorescence intensity of each channel in the region of interest was calculated by subtracting the background adjacent to the ROI. Consequently, the ratio (R) YFP/CFP was calculated. The average R of the 10 seconds before touch was considered R_0. R/R_0 was then plotted to visualize chloride changes during touch stimulation. The R/R_0 change ($\Delta R/R_0$) was calculated as the difference between the average R/R_0 of the last 10 seconds of the recording (Fig. 3C-D during B) and the 10 seconds before touch (Fig. 3C-D during A).

Behavioral assays

Nose touch.: Assays were performed essentially as previously described (Hart et al., 1999). Worms were placed on plates containing a thin layer of bacteria and allowed to recover for 30 minutes. An eyelash hair glued to a toothpick or a glass probe (Fig. S2H-I and K) were placed in front of a forward-moving animal. The responses were recorded as reversals if the worm moved backwards or as head withdraw if the worm moved the head away from the eyelash. No response was noted when the worm continued its forward movement to crawl under, above, or along the eyelash (Kindt et al., 2007). Nose-touch insensitive *deg-1* and *trpa-1* mutants were used as controls (Hart et al., 1999, Kindt et al., 2007). Each worm was tested for 5 consecutive times with a ~30 seconds or ~2 minutes (Fig. S2G and J) interval. At least 10 worms per strain were tested in each assay. The average response (reversals + head withdraw) of each worm to the 5 touches was then used to calculate the average response of each strain. Each mean behavioral response was also plotted for the five touches. *unc-25* worms treated with bicuculline showed a slight uncoordinated phenotype that did not affect their testability for nose touch behaviors.

Osmotic avoidance.: An 8M glycerol ring (1 cm in diameter) was created in the middle of a NGM plate without food, as previously described (Colbert and Bargmann, 1995). Twenty worms per experiment were washed from bacteria and placed inside the ring. After

9 minutes, the percentage of worms that remained inside the ring was calculated. *osm-9* mutants were used as negative control (Colbert et al., 1997).

Octanol avoidance.: An eyelash hair glued to a toothpick was dipped in 10% octanol (in ethanol) and placed in front of a moving forward animal, as previously described (Troemel et al., 1995). The time the animal took to start backward movement was recorded. At least 10 worms per experiment were tested. Adaptation to octanol was assayed following standard procedures (Duan et al., 2020). Five μL of 100% octanol were added to the middle of the lid of a 3 cm diameter NGM plate; consequently, thirty worms were transferred into the plate. The dish was then sealed with parafilm and incubated for 5 minutes at room temperature. After 5 mins exposure, the lid was removed, and the worms were washed with M9 buffer twice. After 30 mins of recovery, at least 10 worms were assayed each time for octanol avoidance as described above. The experiments were repeated twice.

Chemotaxis assays.: Chemotaxis assays were performed as previously described (Coburn and Bargmann, 1996, Roayaie et al., 1998). A chunk of agar 1 cm in diameter was removed from plates and soaked in the attractant (0.2 M Na-acetate) for 3 h. Chunks were put back in the plate overnight to allow equilibration and formation of a gradient. For isoamyl alcohol (1:100 in ethanol) and diacetyl (1:1000 in ethanol) assays, 3 μl of odor at the indicated dilution was placed on one side of the plate, 3 μl of ethanol was placed on the other side of the plate. Thirty worms were then placed on the midline between the test spot and a control spot on the opposite side of the plate. Fifty microliters of 100 mM NaN_3 were placed on both spots to anesthetize animals once they reached the spot. After 1 h, animals on each side of the plate were counted and an attraction index was determined as follows: (number of animals at attractant – number of animals at control) / (number of animals at attractant + number of animals at control). For octanol, isoamyl alcohol, and Na-acetate, *tax-2(p691)* mutant worms were used as negative controls, while *odr-3(n2150)* mutants were used for diacetyl assays (Coburn and Bargmann, 1996, Roayaie et al., 1998).

Worm preparation for supplemented plates experiments—Egg collection was done as previously reported (Porta-de-la-Riva et al., 2012). In brief, plates containing gravid adults were washed using M9 buffer and worms were collected in tubes for centrifugation (4300 rpm for 5 minutes). The pelleted worms were then resuspended in a 400 μl solution containing 22.7% bleach and 0.1 M NaOH and incubated at room temperature for ~5 minutes. When ~90% of the eggs were released, 14 ml of M9 buffer was added to the tube. Eggs were centrifuged and washed twice with M9 before being resuspended in the same buffer and seeded onto supplemented plates.

Plates supplementation and pharmacology—NGM plates supplemented with osmolytes were prepared as previously described (Johnson et al., 2020, Singhvi et al., 2016). The sterile stock solutions of the solutes were dissolved in the liquid NGM to achieve the desired concentrations before being poured into Petri dishes, which were then seeded with *E. coli*. We observed that bacterial growth on plates supplemented with $KHCO_3$ was slow compared to standard NGM plates. To avoid differences in food availability across different conditions, bacteria were concentrated and plated as a thick layer, as previously reported (Johnson et al., 2020).

For nose touch and calcium imaging experiments using bicuculline, 100 µl of a stock solution (10 mM in chloroform) was spread on unseeded NGM plates for a final concentration of 10 µM (Duan et al., 2020). Once the solution was dry, a thin layer of bacteria was seeded and allowed to dry. Worms were then transferred to the plate and allowed to crawl for 30 minutes prior to the assays. Control plates were prepared the same way except that water was used instead of bicuculline. Worms treated with bicuculline showed a slight uncoordinated phenotype that did not affect their testability for nose touch behaviors. For nose touch experiments using forskolin, 1.6 µl of a stock solution (12.5 mM in DMSO) was diluted in 2 ml M9 buffer containing OP50 (6 mg/ml) for a final concentration of 10 µM (Ghosh-Roy et al., 2010). Worms were transferred into this solution and incubated for 2 hours at 20 °C. Finally, treated worms were transferred onto an assay plate. For control worms, water was used instead of forskolin.

Experimental design—All experiments, unless otherwise stated, were performed at least in triplicate with a minimum of three biological replicates, as indicated in figure legends. No strategy for randomization and/or stratification was followed. Behavioral experiments were performed blind to genotype and condition. The sample-size estimation and statistical method of computation were determined by the experiment’s reproducibility and are similar to those generally used in the field, as previously reported (Fay and Gerow, 2013, Duan et al., 2020, Johnson et al., 2020). All the acquired data was included in the analysis and no exclusion criteria was followed.

QUANTIFICATION AND STATISTICAL ANALYSIS

Data and statistical analyses were performed using GraphPad Prism or Clampfit (for calcium transient’s decay times) software, as stated in their corresponding sections. All data is presented as mean ± SEM, and unpaired two-tailed Student’s t test or one-way ANOVA, followed by Tukey’s correction for pairwise comparisons, was used for statistical comparisons. The specific tests used, the n size and type, and the p-values ($p<0.05$ was considered statistically significant) are indicated in the figure legends. No methods were used to determine the statistical approach as only statistical methods generally used in this field were used.

All cartoon figures were created with BioRender.com.

Supplementary Material

Refer to Web version on PubMed Central for supplementary material.

ACKNOWLEDGMENTS

We thank Andrew Fire, Shohei Mitani, William R. Schafer, Michael Push, David M. Miller, Hirofumi Kunitomo, Sreekanth H. Chalasani, and Kenneth G. Miller for sharing DNA plasmids. We thank the Caenorhabditis Genetic Center for strains. We thank Shumin Duan and Lijun Kang for sharing strains ST2499 and ST2181. We thank Stephen Roper, Rong Grace Zhai, Robert W. Kean, Kevin Collins, Hans Peter Larsson, Karl L. Magleby, and

Gerhard Dahl for sharing equipment essential to data collection in this paper. We thank Kevin Collins for critical reading of the manuscript. This work was supported by NIH Grants R01s NS070969 and NS105616A1.

References

ALTUN ZF & HALL DH 2010. Nervous system, neuronal support cells. WormAtlas.

ARREOLA J, BEGENISICH T & MELVIN JE 2002. Conformation-dependent regulation of inward rectifier chloride channel gating by extracellular protons. J Physiol, 541, 103–12. [PubMed: 12015423]

BACAJ T, TEVLIN M, LU Y & SHAHAM S 2008. Glia are essential for sensory organ function in C. elegans. Science, 322, 744–7. [PubMed: 18974354]

BARGMANN CI, THOMAS JH & HORVITZ HR 1990. Chemosensory cell function in the behavior and development of Caenorhabditis elegans. Cold Spring Harb Symp Quant Biol, 55, 529–38. [PubMed: 2132836]

BLANZ J, SCHWEIZER M, AUBERSON M, MAIER H, MUENSCHER A, HUBNER CA & JENTSCH TJ 2007. Leukoencephalopathy upon disruption of the chloride channel ClC-2. J Neurosci, 27, 6581–9. [PubMed: 17567819]

BOSL MR, STEIN V, HUBNER C, ZDEBIK AA, JORDT SE, MUKHOPADHYAY AK, DAVIDOFF MS, HOLSTEIN AF & JENTSCH TJ 2001. Male germ cells and photoreceptors, both dependent on close cell-cell interactions, degenerate upon ClC-2 Cl(−) channel disruption. EMBO J, 20, 1289–99. [PubMed: 11250895]

BRANICKY R, MIYAZAKI H, STRANGE K & SCHAFER WR 2014. The voltage-gated anion channels encoded by clh-3 regulate egg laying in C. elegans by modulating motor neuron excitability. J Neurosci, 34, 764–75. [PubMed: 24431435]

BRENNER S 1974. The genetics of Caenorhabditis elegans. Genetics, 77, 71–94. [PubMed: 4366476]

CELOTTO L, EROLI F, NISTRI A & VILOTTI S 2019. Long-term application of cannabinoids leads to dissociation between changes in cAMP and modulation of GABAA receptors of mouse trigeminal sensory neurons. Neurochem Int, 126, 74–85. [PubMed: 30633953]

CHARLIE NK, THOMURE AM, SCHADE MA & MILLER KG 2006. The Dunce cAMP phosphodiesterase PDE-4 negatively regulates G alpha(s)-dependent and G alpha(s)-independent cAMP pools in the Caenorhabditis elegans synaptic signaling network. Genetics, 173, 111–30. [PubMed: 16624912]

CHEN TW, WARDILL TJ, SUN Y, PULVER SR, RENNINGER SL, BAOHAN A, SCHREITER ER, KERR RA, ORGER MB, JAYARAMAN V, LOOGER LL, SVOBODA K & KIM DS 2013. Ultrasensitive fluorescent proteins for imaging neuronal activity. Nature, 499, 295–300. [PubMed: 23868258]

COBURN CM & BARGMANN CI 1996. A putative cyclic nucleoti-degated channel is required for sensory development and function in C. elegans. Neuron, 17, 695–706. [PubMed: 8893026]

COLBERT HA & BARGMANN CI 1995. Odorant-specific adaptation pathways generate olfactory plasticity in C. elegans. Neuron, 14, 803–12. [PubMed: 7718242]

COLBERT HA, SMITH TL & BARGMANN CI 1997. OSM-9, a novel protein with structural similarity to channels, is required for olfaction, mechanosensation, and olfactory adaptation in Caenorhabditis elegans. J Neurosci, 17, 8259–69. [PubMed: 9334401]

CONSORTIUM, C. E. D. M. 2012. large-scale screening for targeted knockouts in the Caenorhabditis elegans genome. G3 (Bethesda), 2, 1415–25. [PubMed: 23173093]

DEPIENNE C, BUGIANI M, DUPUITS C, GALANAUD D, TOUITOU V, POSTMA N, VAN BERKEL C, POLDER E, TOLLARD E, DARIOS F, BRICE A, DE DIE-SMULDERS CE, VLES JS, VANDERVER A, UZIEL G, YALCINKAYA C, FRINTS SG, KALSCHEUER VM, KLOOSTER J, KAMERMANS M, ABBINK TE, WOLF NI, SEDEL F & VAN DER KNAAP MS 2013. Brain white matter oedema due to ClC-2 chloride channel deficiency: an observational analytical study. Lancet Neurol, 12, 659–68. [PubMed: 23707145]

DING G, ZOU W, ZHANG H, XUE Y, CAI Y, HUANG G, CHEN L, DUAN S & KANG L 2015. In vivo tactile stimulation-evoked responses in Caenorhabditis elegans amphid sheath glia. PLoS One, 10, e0117114. [PubMed: 25671616]

DUAN D, ZHANG H, YUE X, FAN Y, XUE Y, SHAO J, DING G, CHEN D, LI S, CHENG H, ZHANG X, ZOU W, LIU J, ZHAO J, WANG L, ZHAO B, WANG Z, XU S, WEN Q, LIU J, DUAN S & KANG L 2020. Sensory Glia Detect Repulsive Odorants and Drive Olfactory Adaptation. Neuron, 108, 707–721 e8. [PubMed: 32970991]

EDELSTEIN AD, TSUCHIDA MA, AMODAJ N, PINKARD H, VALE RD & STUURMAN N 2014. Advanced methods of microscope control using muManager software. J Biol Methods, 1.

ESPOSITO G, DI SCHIAVI E, BERGAMASCO C & BAZZICALUPO P 2007. Efficient and cell specific knock-down of gene function in targeted C. elegans neurons. Gene, 395, 170–6. [PubMed: 17459615]

FARRANT M & NUSSER Z 2005. Variations on an inhibitory theme: phasic and tonic activation of GABA(A) receptors. Nat Rev Neurosci, 6, 215–29. [PubMed: 15738957]

FAY DS & GEROW K 2013. A biologist's guide to statistical thinking and analysis. WormBook, 1–54.

GEFFENEY SL, CUEVA JG, GLAUSER DA, DOLL JC, LEE TH, MONTOYA M, KARANIA S, GARAKANI AM, PRUITT BL & GOODMAN MB 2011. DEG/ENaC but not TRP channels are the major mechanoelectrical transduction channels in a C. elegans nociceptor. Neuron, 71, 845–57. [PubMed: 21903078]

GHOSH-ROY A, WU Z, GONCHAROV A, JIN Y & CHISHOLM AD 2010. Calcium and cyclic AMP promote axonal regeneration in Caenorhabditis elegans and require DLK-1 kinase. J Neurosci, 30, 3175–83. [PubMed: 20203177]

GOODMAN MB & SENGUPTA P 2019. How Caenorhabditis elegans Senses Mechanical Stress, Temperature, and Other Physical Stimuli. Genetics, 212, 25–51. [PubMed: 31053616]

GRANT J, MATTHEWMAN C & BIANCHI L 2015. A Novel Mechanism of pH Buffering in C. elegans Glia: Bicarbonate Transport via the Voltage-Gated ClC Cl− Channel CLH-1. J Neurosci, 35, 16377–97. [PubMed: 26674864]

HALLS ML & COOPER DM 2011. Regulation by Ca2+-signaling pathways of adenylyl cyclases. Cold Spring Harb Perspect Biol, 3, a004143. [PubMed: 21123395]

HAN L, WANG Y, SANGALETTI R, D'URSO G, LU Y, SHAHAM S & BIANCHI L 2013. Two novel DEG/ENaC channel subunits expressed in glia are needed for nose-touch sensitivity in Caenorhabditis elegans. J Neurosci, 33, 936–49. [PubMed: 23325233]

HARRIS G, MILLS H, WRAGG R, HAPIAK V, CASTELLETTO M, KORCHNAK A & KOMUNIECKI RW 2010. The monoaminergic modulation of sensory-mediated aversive responses in Caenorhabditis elegans requires glutamatergic/peptidergic cotransmission. J Neurosci, 30, 7889–99. [PubMed: 20534837]

HART AC, KASS J, SHAPIRO JE & KAPLAN JM 1999. Distinct signaling pathways mediate touch and osmosensory responses in a polymodal sensory neuron. J Neurosci, 19, 1952–8. [PubMed: 10066248]

HE S, CUENTAS-CONDORI A & MILLER DM 3RD 2019. NATF (Native and Tissue-Specific Fluorescence): A Strategy for Bright, Tissue-Specific GFP Labeling of Native Proteins in Caenorhabditis elegans. Genetics, 212, 387–395. [PubMed: 30952669]

HEIMAN MG & SHAHAM S 2009. DEX-1 and DYF-7 establish sensory dendrite length by anchoring dendritic tips during cell migration. Cell, 137, 344–55. [PubMed: 19344940]

HORI S, ODA S, SUEHIRO Y, IINO Y & MITANI S 2018. OFF-responses of interneurons optimize avoidance behaviors depending on stimulus strength via electrical synapses. PLoS Genet, 14, e1007477. [PubMed: 29939997]

HOU X, ZHANG R, WANG J, LI Y, LI F, ZHANG Y, ZHENG X, SHEN Y, WANG Y & ZHOU L 2018. CLC-2 is a positive modulator of oligodendrocyte precursor cell differentiation and myelination. Mol Med Rep, 17, 4515–4523. [PubMed: 29344669]

IKEDA R, CHA M, LING J, JIA Z, COYLE D & GU JG 2014. Merkel cells transduce and encode tactile stimuli to drive Abeta-afferent impulses. Cell, 157, 664–75. [PubMed: 24746027]

JOHNSON CK, FERNANDEZ-ABASCAL J, WANG Y, WANG L & BIANCHI L 2020. The Na(+)-K(+)-ATPase is needed in glia of touch receptors for responses to touch in C. elegans. J Neurophysiol, 123, 2064–2074. [PubMed: 32292107]

KAPLAN JM & HORVITZ HR 1993. A dual mechanosensory and chemosensory neuron in Caenorhabditis elegans. Proc Natl Acad Sci U S A, 90, 2227–31. [PubMed: 8460126]

KATO S, XU Y, CHO CE, ABBOTT LF & BARGMANN CI 2014. Temporal responses of C. elegans chemosensory neurons are preserved in behavioral dynamics. Neuron, 81, 616–28. [PubMed: 24440227]

KINDT KS, VISWANATH V, MACPHERSON L, QUAST K, HU H, PATAPOUTIAN A & SCHAFER WR 2007. Caenorhabditis elegans TRPA-1 functions in mechanosensation. Nat Neurosci, 10, 568–77. [PubMed: 17450139]

KOMATSU H, MORI I, RHEE JS, AKAIKE N & OHSHIMA Y 1996. Mutations in a cyclic nucleotide-gated channel lead to abnormal thermosensation and chemosensation in C. elegans. Neuron, 17, 707–18. [PubMed: 8893027]

KRZYZANOWSKI MC, WOLDEMARIAM S, WOOD JF, CHAUBEY AH, BRUEGGEMANN C, BOWITCH A, BETHKE M, L'ETOILE ND & FERKEY DM 2016. Aversive Behavior in the Nematode C. elegans Is Modulated by cGMP and a Neuronal Gap Junction Network. PLoS Genet, 12, e1006153. [PubMed: 27459302]

KWAK H, KOH W, KIM S, SONG K, SHIN JI, LEE JM, LEE EH, BAE JY, HA GE, OH JE, PARK YM, KIM S, FENG J, LEE SE, CHOI JW, KIM KH, KIM YS, WOO J, LEE D, SON T, KWON SW, PARK KD, YOON BE, LEE J, LI Y, LEE H, BAE YC, LEE CJ & CHEONG E 2020. Astrocytes Control Sensory Acuity via Tonic Inhibition in the Thalamus. Neuron, 108, 691–706 e10. [PubMed: 32905785]

LEE RY, SAWIN ER, CHALFIE M, HORVITZ HR & AVERY L 1999. EAT-4, a homolog of a mammalian sodium-dependent inorganic phosphate cotransporter, is necessary for glutamatergic neurotransmission in caenorhabditis elegans. J Neurosci, 19, 159–67. [PubMed: 9870947]

LEE S, YOON BE, BERGLUND K, OH SJ, PARK H, SHIN HS, AUGUSTINE GJ & LEE CJ 2010. Channel-mediated tonic GABA release from glia. Science, 330, 790–6. [PubMed: 20929730]

LIU J, WARD A, GAO J, DONG Y, NISHIO N, INADA H, KANG L, YU Y, MA D, XU T, MORI I, XIE Z & XU XZ 2010. C. elegans phototransduction requires a G protein-dependent cGMP pathway and a taste receptor homolog. Nat Neurosci, 13, 715–22. [PubMed: 20436480]

LIU Z, KARIYA MJ, CHUTE CD, PRIBADI AK, LEINWAND SG, TONG A, CURRAN KP, BOSE N, SCHROEDER FC, SRINIVASAN J & CHALASANI SH 2018. Predator-secreted sulfolipids induce defensive responses in C. elegans. Nat Commun, 9, 1128. [PubMed: 29555902]

LOLIGNIER S, EIJKELKAMP N & WOOD JN 2015. Mechanical allodynia. Pflugers Arch, 467, 133–9. [PubMed: 24846747]

MA BF, XIE MJ & ZHOU M 2012. Bicarbonate efflux via GABA(A) receptors depolarizes membrane potential and inhibits two-pore domain potassium channels of astrocytes in rat hippocampal slices. Glia, 60, 1761–72. [PubMed: 22855415]

MELLO CC, KRAMER JM, STINCHCOMB D & AMBROS V 1991. Efficient gene transfer in C.elegans: extrachromosomal maintenance and integration of transforming sequences. EMBO J, 10, 3959–70. [PubMed: 1935914]

NIKOLAEV YA, FEKETA VV, ANDERSON EO, SCHNEIDER ER, GRACHEVA EO & BAGRIANTSEV SN 2020. Lamellar cells in Pacinian and Meissner corpuscles are touch sensors. Sci Adv, 6.

PARK C, SAKURAI Y, SATO H, KANDA S, IINO Y & KUNITOMO H 2021. Roles of the ClC chloride channel CLH-1 in food-associated salt chemotaxis behavior of C. elegans. Elife, 10.

PAWSON L, PRESTIA LT, MAHONEY GK, GUCLU B, COX PJ & PACK AK 2009. GABAergic/glutamatergic-glial/neuronal interaction contributes to rapid adaptation in pacinian corpuscles. J Neurosci, 29, 2695–705. [PubMed: 19261864]

PERENS EA & SHAHAM S 2005. C. elegans daf-6 encodes a patched-related protein required for lumen formation. Dev Cell, 8, 893–906. [PubMed: 15935778]

PIGGOTT BJ, LIU J, FENG Z, WESCOTT SA & XU XZ 2011. The neural circuits and synaptic mechanisms underlying motor initiation in C. elegans. Cell, 147, 922–33. [PubMed: 22078887]

PLAZAOLA-SASIETA H, ZHU Q, GAITAN-PENAS H, RIOS M, ESTEVEZ R & MOREY M 2019. Drosophila ClC-a is required in glia of the stem cell niche for proper neurogenesis and wiring of neural circuits. Glia, 67, 2374–2398. [PubMed: 31479171]

PORTA-DE-LA-RIVA M, FONTRODONA L, VILLANUEVA A & CERON J 2012. Basic Caenorhabditis elegans methods: synchronization and observation. J Vis Exp, e4019. [PubMed: 22710399]

PUTS NA, HARRIS AD, CROCETTI D, NETTLES C, SINGER HS, TOMMERDAHL M, EDDEN RA & MOSTOFSKY SH 2015. Reduced GABAergic inhibition and abnormal sensory symptoms in children with Tourette syndrome. J Neurophysiol, 114, 808–17. [PubMed: 26041822]

ROAYAIE K, CRUMP JG, SAGASTI A & BARGMANN CI 1998. The G alpha protein ODR-3 mediates olfactory and nociceptive function and controls cilium morphogenesis in C. elegans olfactory neurons. Neuron, 20, 55–67. [PubMed: 9459442]

RUTLEDGE E, BIANCHI L, CHRISTENSEN M, BOEHMER C, MORRISON R, BROSLAT A, BELD AM, GEORGE AL, GREENSTEIN D & STRANGE K 2001. CLH-3, a ClC-2 anion channel ortholog activated during meiotic maturation in C. elegans oocytes. Curr Biol, 11, 161–70. [PubMed: 11231150]

SAINT-MARTIN C, GAUVAIN G, TEODORESCU G, GOURFINKEL-AN I, FEDIRKO E, WEBER YG, MALJEVIC S, ERNST JP, GARCIA-OLIVARES J, FAHLKE C, NABBOUT R, LEGUERN E, LERCHE H, PONCER JC & DEPIENNE C 2009. Two novel CLCN2 mutations accelerating chloride channel deactivation are associated with idiopathic generalized epilepsy. Hum Mutat, 30, 397–405. [PubMed: 19191339]

SCHADE MA, REYNOLDS NK, DOLLINS CM & MILLER KG 2005. Mutations that rescue the paralysis of Caenorhabditis elegans ric-8 (synembryn) mutants activate the G alpha(s) pathway and define a third major branch of the synaptic signaling network. Genetics, 169, 631–49. [PubMed: 15489510]

SCHAFER WR 2015. Mechanosensory molecules and circuits in C. elegans. Pflugers Arch, 467, 39–48. [PubMed: 25053538]

SIK A, SMITH RL & FREUND TF 2000. Distribution of chloride channel-2-immunoreactive neuronal and astrocytic processes in the hippocampus. Neuroscience, 101, 51–65. [PubMed: 11068136]

SINGHVI A, LIU B, FRIEDMAN CJ, FONG J, LU Y, HUANG XY & SHAHAM S 2016. A Glial K/Cl Transporter Controls Neuronal Receptive Ending Shape by Chloride Inhibition of an rGC. Cell, 165, 936–48. [PubMed: 27062922]

SUZUKI H, KERR R, BIANCHI L, FROKJAER-JENSEN C, SLONE D, XUE J, GERSTBREIN B, DRISCOLL M & SCHAFER WR 2003. In vivo imaging of C. elegans mechanosensory neurons demonstrates a specific role for the MEC-4 channel in the process of gentle touch sensation. Neuron, 39, 1005–17. [PubMed: 12971899]

TROEMEL ER, CHOU JH, DWYER ND, COLBERT HA & BARGMANN CI 1995. Divergent seven transmembrane receptors are candidate chemosensory receptors in C. elegans. Cell, 83, 207–18. [PubMed: 7585938]

WANG Y, APICELLA A JR., LEE SK, EZCURRA M, SLONE RD, GOLDMIT M, SCHAFER WR, SHAHAM S, DRISCOLL M & BIANCHI L 2008. A glial DEG/ENaC channel functions with neuronal channel DEG-1 to mediate specific sensory functions in C. elegans. EMBO J, 27, 2388–99. [PubMed: 18701922]

WANG Y, D'URSO G & BIANCHI L 2012. Knockout of glial channel ACD-1 exacerbates sensory deficits in a C. elegans mutant by regulating calcium levels of sensory neurons. J Neurophysiol, 107, 148–58. [PubMed: 21994266]

WEI J, ZHAO AZ, CHAN GC, BAKER LP, IMPEY S, BEAVO JA & STORM DR 1998. Phosphorylation and inhibition of olfactory adenylyl cyclase by CaM kinase II in Neurons: a mechanism for attenuation of olfactory signals. Neuron, 21, 495–504. [PubMed: 9768837]

WOO SH, RANADE S, WEYER AD, DUBIN AE, BABA Y, QIU Z, PETRUS M, MIYAMOTO T, REDDY K, LUMPKIN EA, STUCKY CL & PATAPOUTIAN A 2014. Piezo2 is required for Merkel-cell mechanotransduction. Nature, 509, 622–6. [PubMed: 24717433]

YUAN A, WANG Z, XU W, DING Q, ZHAO Y, HAN J & SUN J 2020. A Rare Novel CLCN2 Variation and Risk of Gilles de la Tourette Syndrome: Whole-Exome Sequencing in a Multiplex Family and a Follow-Up Study in a Chinese Population. Front Psychiatry, 11, 543911. [PubMed: 33343406]

ZHU GQ, LIU S, HE DD, LIU YP & SONG XJ 2014. Activation of the cAMP-PKA signaling pathway in rat dorsal root ganglion and spinal cord contributes toward induction and maintenance of bone cancer pain. Behav Pharmacol, 25, 267–76. [PubMed: 24978483]

ZOU W, FU J, ZHANG H, DU K, HUANG W, YU J, LI S, FAN Y, BAYLIS HA, GAO S, XIAO R, JI W, KANG L & XU T 2018. Decoding the intensity of sensory input by two glutamate receptors in one C. elegans interneuron. Nat Commun, 9, 4311. [PubMed: 30333484]

Highlights

- CLH-1 is needed in AMsh glia for touch responses and for ASH neurons' adaptation.
- GABA signaling from AMsh glia is required for touch behavior and ASH adaptation.
- CLH-1 mediates Cl^- efflux from AMsh glia required for GABA signaling.
- CLH-1 is also required for cAMP signaling in ASH neurons needed for touch responses.

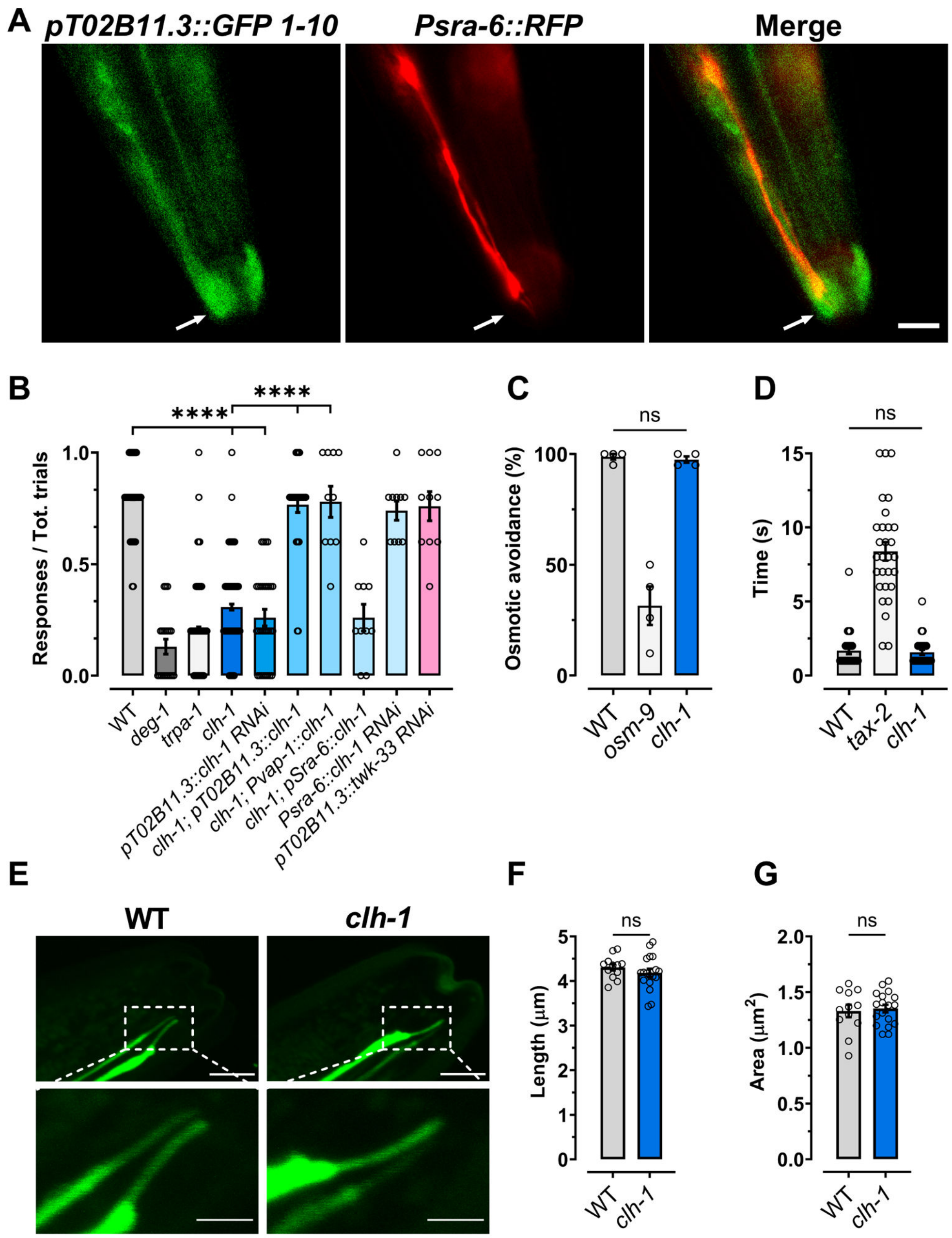

Fig. 1. CLH-1 in needed in amphid glia for nose touch responses.

(A) Representative images of a worm expressing *GFP11$_{X7}$::clh-1* knock-in, *pT02B11.3::GFP1-10*, and *Psra-6::RFP* taken with GFP (left) and RFP (middle) filters. The panel on the right is a merge of the first two panels. Arrows indicate the position of the sensory cilia. Scale bar: 5 µm. (B) *clh-1(ok658)* knockout worms are nose touch insensitive. The nose touch insensitivity is rescued by expression of *clh-1* cDNA under the control of AMsh glia specific promoters T02B11.3 and *vap-1* (Bacaj et al., 2008, Perens and Shaham, 2005), but not under the control of ASH neurons' promoter *sra-6* (Troemel et al., 1995). Nose touch insensitivity is also observed in animals in which *clh-1* is knocked down in AMsh glia by RNAi, but not in animals in which *clh-1* is knocked down in ASH

Author Manuscript

Author Manuscript

Author Manuscript

neurons, and in which unrelated *twk-33* gene is knocked down in AMsh glia. Nose touch insensitive *deg-1(u38u421)* and *trpa-1(ok999)* mutants are the negative controls. Each data point represents one worm (n = 270, 20, 270, 210, 30, 30, 10, 10, 10 and 10, respectively). **(C)** Knockout of *clh-1* does not alter osmotic avoidance behavior in *C. elegans*. Each data point represents an independent experiment (n = 4) in which at least 20 worms each were tested. **(D)** The octanol avoidance response is normal in *clh-1(ok658)* mutant worms. Each data point represents one worm (n = 28, 29 and 30, respectively). **(E)** Representative images of the ASH cilia in wild type (left panels) and *clh-1(ok658)* (right panels) worms. Bottom panels are insets of the top panels (dashed square box). Scale bar: 2 µm. **(F-G)** *clh-1* knockout does not alter the length **(F)** or the area **(G)** of the sensory cilia in ASH neurons. Each data point represents one worm (WT, n = 12; *clh-1*, n = 18). **B-D**, **F**, **G**: Columns represent mean ± SEM. Statistics were calculated by one-way ANOVA followed by Tukey post-test (ns, not significant (p>0.05); ****p<0.0001) for panels **B**, **C**, and **D**, and by two-tailed unpaired t-Test for panels **F** and **G**.

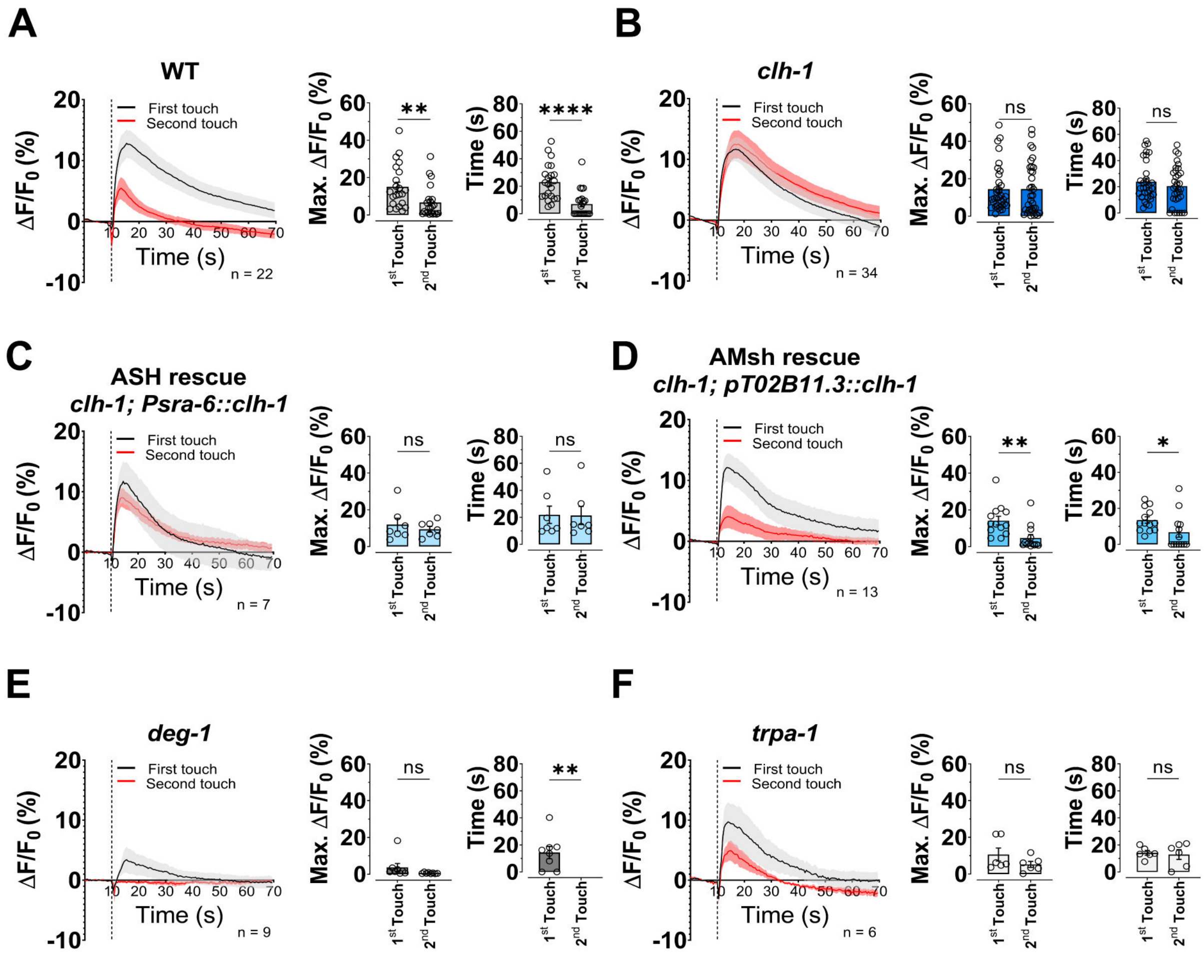

Fig. 2. ASH neurons' adaptation to touch is mediated by glial CLH-1.

(A-F) Left panels, calcium transients generated in ASH neurons by two nose touch stimulations as measured by % increase of GCaMP-6s fluorescence above the baseline (ΔF/F) in wild type **(A)**, *clh-1(ok658)* **(B)**, CLH-1 rescue in ASH neurons **(C)**, CLH-1 rescue in AMsh glia **(D)**, *deg-1(u38u421)* **(E)**, and *trpa-1(ok999)* **(F)** worms. Data are shown as mean ± SEM (light gray and red). The first touch is shown in black, the second in red. The number of animals tested is shown within each panel. The vertical dashed line shows when the touch stimulation was delivered. Middle panels, peak percentage (%) of GCaMP-6s ΔF/F. Right panels, GCaMP-6s fluorescence decay time constants. Individual data points are shown as open circles and columns represent mean ± SEM. Statistics were calculated by two-tailed unpaired t-Test (ns, not significant ($p>0.05$), *$p<0.05$, **$p<0.01$, ****$p<0.0001$).

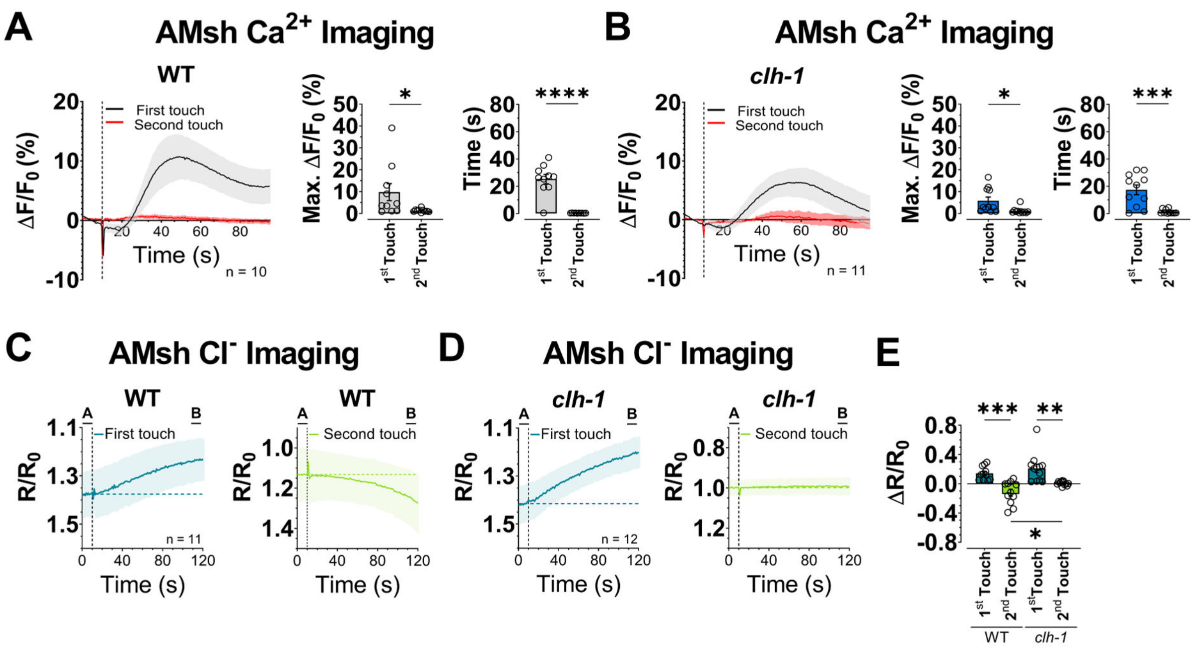

Fig. 3. CLH-1 mediates Cl^- efflux upon touch stimulation.

(A-B) Left panels, Calcium transients generated in AMsh glia by two nose touch stimulations as measured by % increase of GCaMP-6s fluorescence above the baseline (ΔF/F) in wild type **(A)** and *clh-1(ok658)* **(B)** worms. Data are shown as mean ± SEM (light gray and red). The first touch is shown in black, the second in red. The number of animals tested is shown within each panel. The vertical dashed line shows when the touch stimulation was delivered. Middle panels, peak percentage (%) of GCaMP-6s ΔF/F. Right panels, GCaMP-6s fluorescence decay time constants. Individual data points are shown as symbols and columns represent mean ± SEM. **(C-D)** Intracellular Cl^- in AMsh glia of wild type **(C)** and *clh-1* knockout **(D)** worms upon touch stimulation as measured by SuperClomeleon fluorescence. Data represent the YFP/CFP ratio (R) change with respect to the baseline (R_0, 10 seconds before touch). Data are mean ± SEM. The number of animals tested is shown in the first touch panel. The vertical dashed line shows when the touch stimulation was delivered. The horizontal dashed line represents the average R/R_0 of the 10 seconds before touch. The left panels with traces in dark green correspond to the first touch, the right panels with traces in light green correspond to the second touch. **(E)** Average R/R_0 change of the last 10 seconds of recording with respect to the baseline (B – A in panels C and D). Data are individual worms (symbols) and mean ± SEM (columns). Statistics were by two-tailed unpaired t-Test (ns, not significant ($p>0.05$), *$p<0.05$, **$p<0.01$, ***$p<0.001$, ****$p<0.0001$). One-way ANOVA followed by Tukey post-test (*$p<0.05$, **$p<0.01$, ***$p<0.001$) was used for panel E.

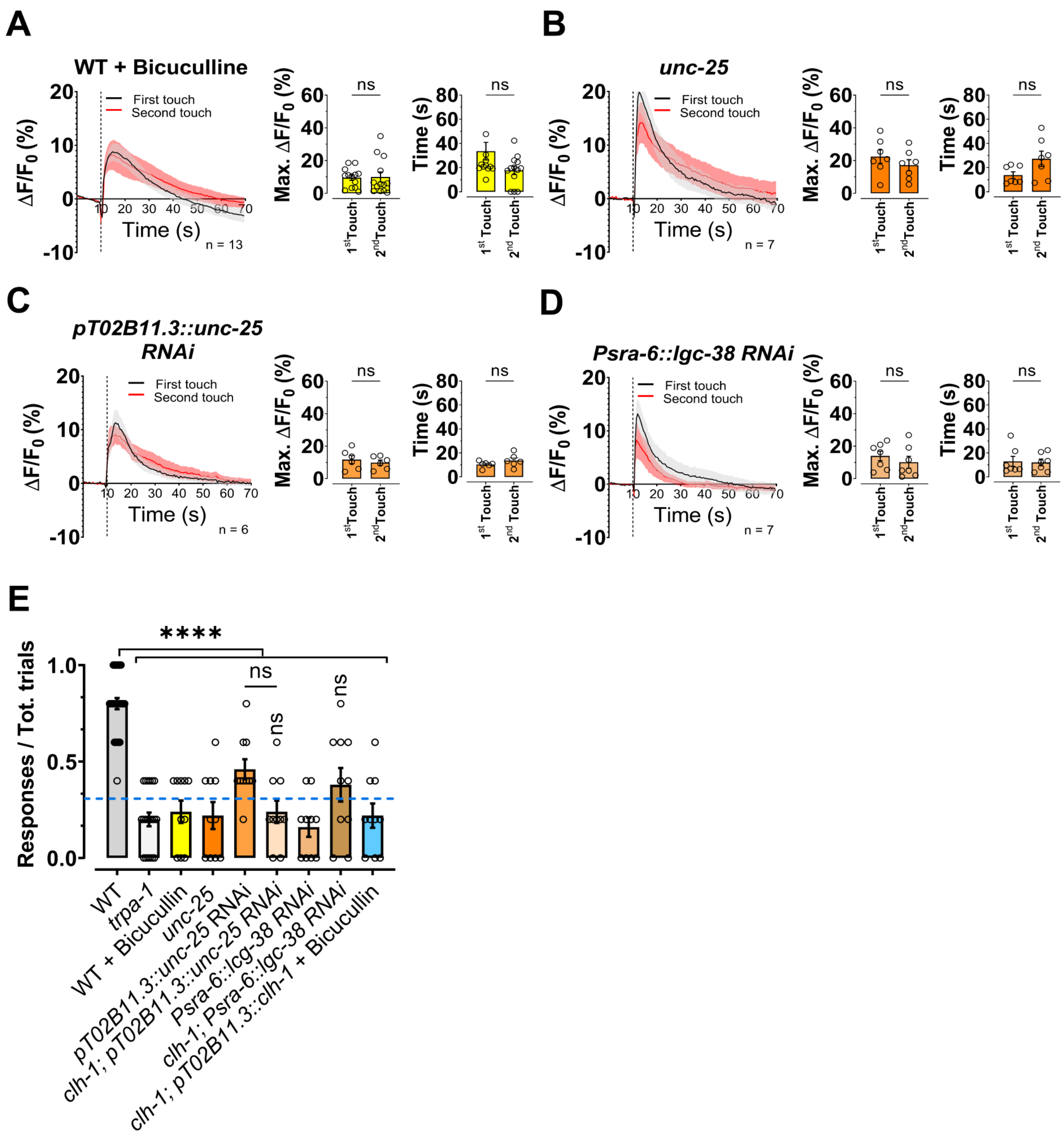

Figure 4. ASH calcium transients' adaptation to touch is mediated by GABA and loss of GABA signaling causes nose touch insensitivity.

(A-D) Left panels, calcium transients in ASH neurons upon two consecutive nose touch stimulations in wild type animals treated with bicuculline **(A)**, in *unc-25(e156)* mutants **(B)**, in animals in which the *unc-25* has been knocked down in AMsh glia **(C)**, in animals in which the $GABA_A$ receptor *lgc-38* has been knocked down in ASH neurons **(D)**. Data are shown as mean ± SEM (light gray and red). The first touch is in black and the second in red, the number of animals tested is shown in each panel. The vertical dashed line is when the touch stimulation was delivered. Middle panels, peak percentage (%) of GCaMP-6s ΔF/F. Right panels, time constants of fluorescence decay. Individual data points are shown as open circles, averages are shown as columns. We note that Ca^{2+} transients in *unc-25* and *lgc-38* RNAi animals are in general faster than in wild type, possibility due to the stronger buffering capacity of GCaMP-5 versus GCaMP-6s (Chen et al., 2013). **(E)** Behavioral nose touch responses for wild type, *trpa-1(ok999),* wild type animals treated with bicuculline, *unc-25(e156)* mutants, *unc-25* AMsh glial RNAi, *clh-1; unc-25* AMsh glial RNAi, animals in which the $GABA_A$ receptor *lgc-38* has been knocked down in ASH neurons, *clh-1; lgc-38 RNAi* in ASH, and *clh-1* AMsh glia rescue treated with bicuculline. Columns represent mean ± SEM and each point represent one worm (n= 30, 20, 10, 10, 10, 10, 10, 10 and 10 respectively). The blue dashed line represents the *clh-1* knockout nose touch response from Fig. 1B. Statistics were calculated using two-tailed unpaired t-Test **(A-D)** or one-way ANOVA followed by Tukey post-test (ns, not significant ($p>0.05$), ****$p<0.0001$) **(E)**. Vertical asterisks in panel E are for statistics *vs clh-1* knockout.

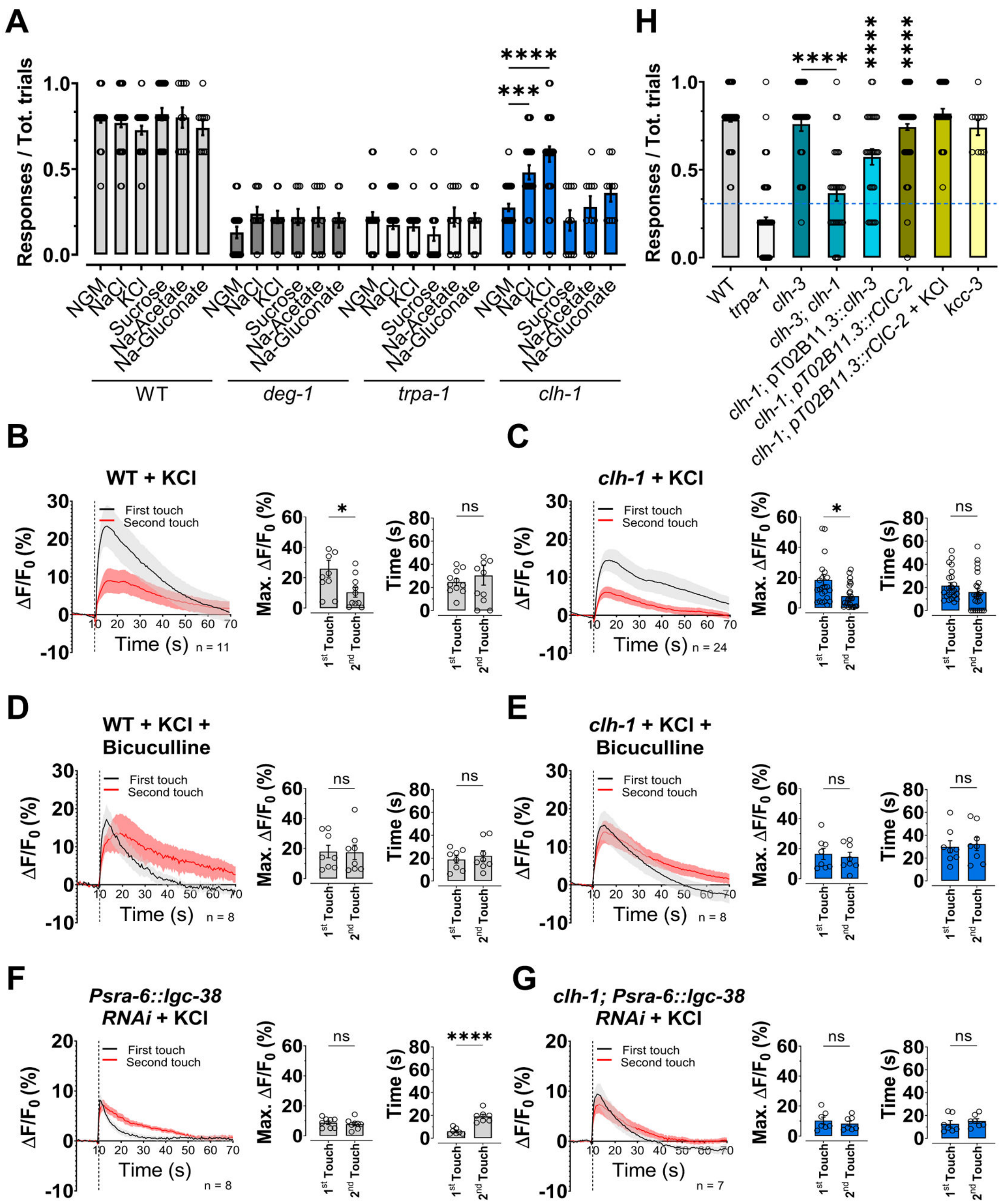

Figure 5. Chloride supplementation rescues nose touch insensitivity of *clh-1* knockout worms.

(A) The nose touch insensitivity of *clh-1* knockout worms is partially rescued by cultivation on plates enriched with 150 mM NaCl or KCl, but not with 300 mM sucrose, or 150 mM Na-acetate or Na-gluconate. Each data point represents one worm (n= 20, 10, 20, and 10, for wild type, *deg-1, trpa-1*, and *clh-1*, respectively). Data are expressed as mean ± SEM (columns). **(B-G)** Left panels, calcium transients upon two consecutive nose touch stimulations in wild type **(B)** and *clh-1(ok658)* **(C)** worms grown in plates supplemented with KCl, wild type **(D)** and *clh-1(ok658)* **(E)** worms grown in plates supplemented with KCl and treated with bicuculline, and wild type **(F)** and *clh-1(ok658)* **(G)** worms knocked-down for *lgc-38* in ASH neurons and grown in plates supplemented with KCl. Data are shown as mean ± SEM (light gray and red), with the first touch shown in black and the second touch shown in red. The number of worms tested is shown in the panels; the vertical dashed line is when the touch stimulation was delivered. Middle panels, peak percentage (%) of GCaMP-6s ΔF/F. Right panels, time constants of fluorescence decay. Individual data points are shown as open circles, averages are shown as columns. **(H)** *clh-1(ok658)* nose touch insensitivity is rescued by expression of worm CLH-3 and rat ClC-2 in AMsh glia. However, *clh-3* is not per se needed for nose touch responses. The K^+/Cl^- cotransporter *kcc-3* is also not needed for nose touch. Each data point represents one worm (n= 180, 180, 30, 30, 30, 120, 30, and 10 respectively). Data are expressed as mean ± SEM (columns). The blue dotted line represents the *clh-1* knockout level (mean from Fig 1B). Statistics were calculated using two-tailed unpaired t-Test (*p<0.05) **(B-G)** or one-way ANOVA followed by Tukey post-test (**<0.01; ***p<0.001; ****p<0.0001) (**A** and **H**). Vertical asterisks indicate comparison with *clh-1* knockout.

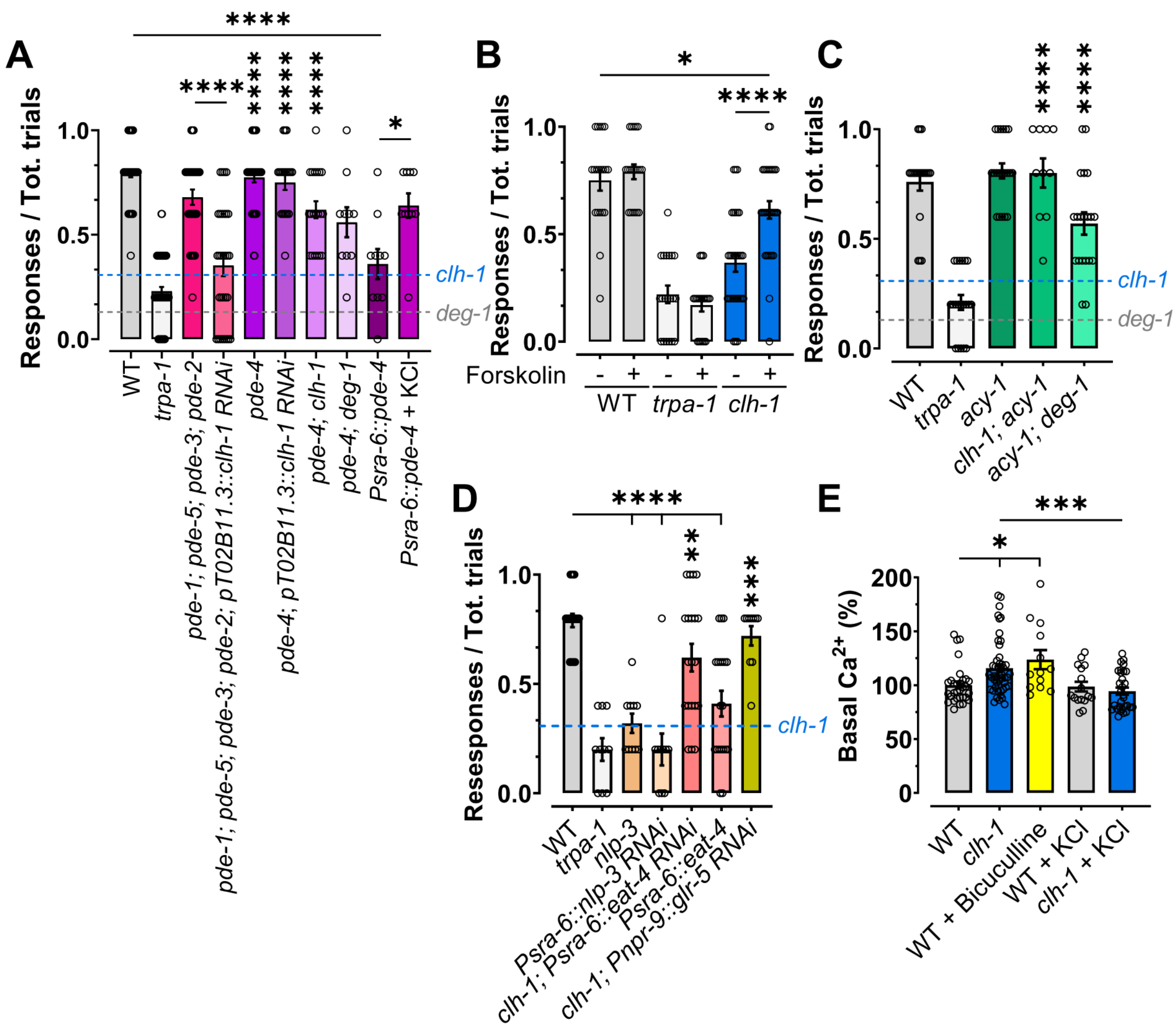

Figure 6. cAMP is a regulator of touch responses in ASH neurons.

(A) Knockout of cAMP specific phosphodiesterase *pde-4* rescues the nose touch insensitive phenotype of *clh-1* knockout, *clh-1* AMsh glia RNAi, and *deg-1* mutant worms. Overexpression in ASH of *pde-4* result in nose touch insensitivity, which is rescued by KCl supplementation. Combined knockout of the cGMP phosphodiesterase genes *pde-1, pde-2, pde-3*, and *pde-5* has no effect on *clh-1* phenotype (n= 60, 60, 30, 30, 40, 20, 20, 10 and 10, respectively). **(B)** Treatment with the activator of adenylyl cyclase forskolin partially rescues the *clh-1* nose touch insensitivity (n= 20 for wild type and *trpa-1*, and 30 for *clh-1*). **(C)** A gain of function mutation in adenylyl cyclase gene *acy-1(md1756)* rescues nose touch insensitivity of *clh-1* knockout worms and partially rescues *deg-1* mutants' nose touch insensitivity (n= 20, 20, 20, 10, and 20, respectively). The dotted lines in panels A, C and D represent the *clh-1* and *deg-1* mutant levels (means from Fig. 1B). **(D)** Global knockout or knock-down in ASH neurons of *nlp-3* and overexpression of *eat-4* causes nose touch insensitivity. Knock-down of *eat-4* in ASH and of *glr-5* in AIB of *clh-1* knockout animals rescue nose touch avoidance. n= 20, 10, 10, 10, 20, 20, and 10, respectively. **(E)** Basal GCaMP-6s fluorescence normalized to the average wild type basal fluorescence in the indicated strains and conditions. n = 31, 49, 13, 16, and 30, respectively. **(A-E)** Columns represent mean ± SEM and each point represent one worm. Statistics were calculated using one-way ANOVA followed by Tukey post-test (ns, not statistical ($p>0.05$); *$p<0.05$; **$p<0.01$; ****<0.0001). Vertical asterisks indicate comparison with their respective controls, either *clh-1* or *deg-1*.

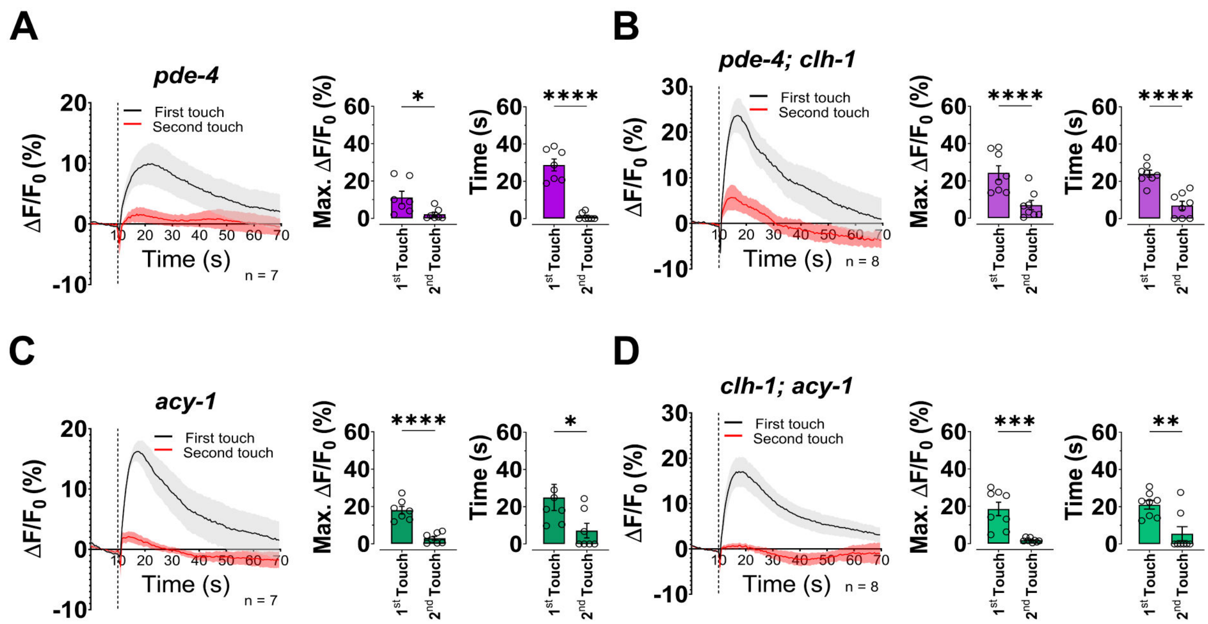

Fig. 7. The adaptation to touch of ASH neurons in *clh-1* worms is rescued by increased cAMP levels.

(A-D) Left panels, calcium transients in in ASH neurons upon two consecutive nose touch stimulations in *pde-4* **(A)**, *pde-4; clh-1* **(B)**, *acy-1* **(C)**, and *clh-1; acy-1* **(D)** worms. Data are shown as mean ± SEM (light gray and red). The first touch is in black and the second in red, the number of animals tested is in each panel. The vertical dashed line is when the touch stimulation was delivered. Middle panels, peak percentage (%) of GCaMP-6s ΔF/F. Right panels, time constants of fluorescence decay. Individual data points are shown as open circles, averages are shown as columns. Data are expressed as mean ± SEM. Statistics were calculated using two-tailed unpaired t-test (*$p<0.05$; **$p<0.01$; ***$p<0.001$; ****$p<0.0001$).

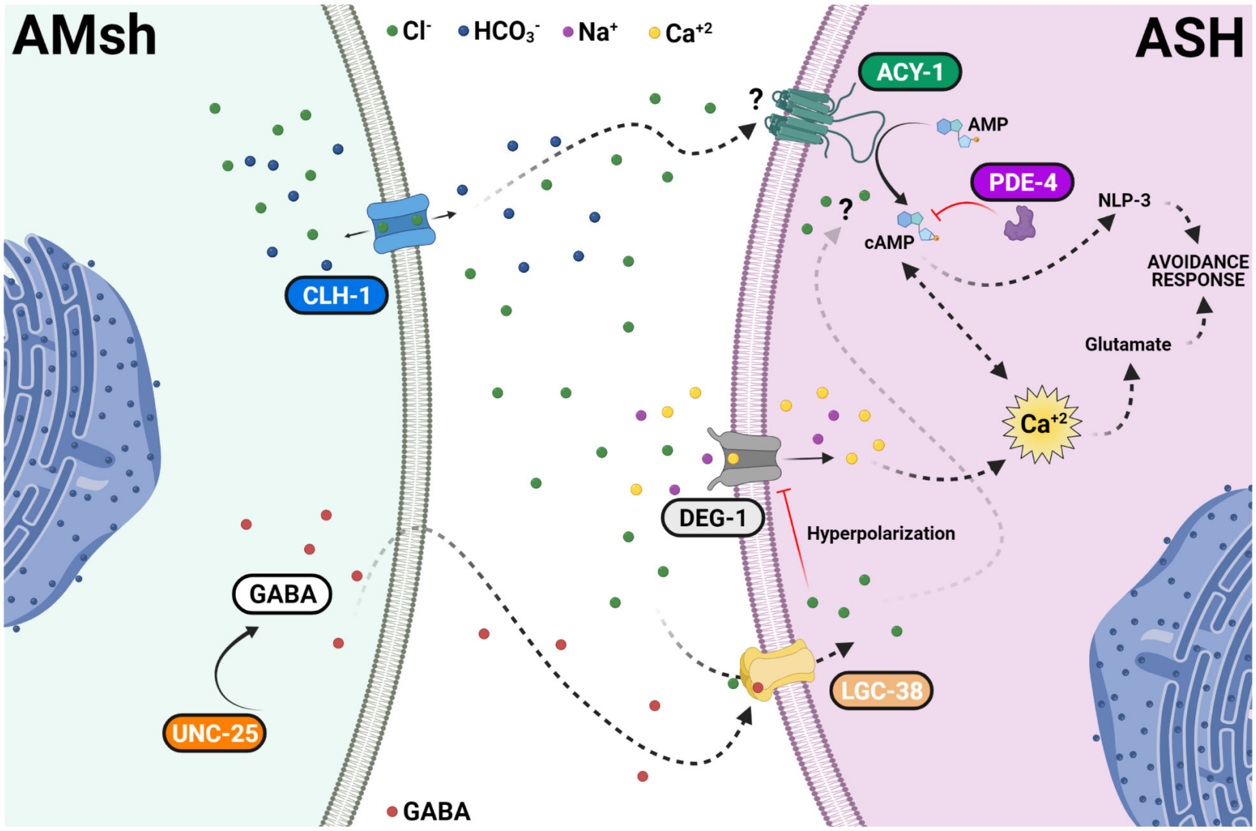

Fig. 8. Regulation of touch neurons' function by glial Cl^{-} channel CLH-1 in *C. elegans*.

Activation of DEG/ENaC channel DEG-1 by mechanical forces causes depolarization of ASH which is expected to activate voltage-gated Ca^{2+} channel EGL-19, leading to elevation of intracellular Ca^{2+} concentrations ($[Ca^{2+}]_i$). Elevation of $[Ca^{2+}]_i$ causes the release of glutamate. CLH-1 is expressed in AMsh glia and mediates Cl^{-} flux needed for GABA signaling. GABA activation of the $GABA_A$ receptor LGC-38 causes hyperpolarization of the ASH touch neuron's plasma membrane. This hyperpolarization closes EGL-19 leading to a decrease in the $[Ca^{2+}]_i$, and thus, in glutamate release. A second pathway involving cAMP synthesis by adenylyl cyclase ACY-1 and degradation by phosphodiesterase PDE-4 is also influenced by AMsh glia CLH-1. This regulation might be either directly mediated by Cl^{-} on the activity of ACY-1 or indirectly mediated by Ca^{2+} inhibition of ACY-1. cAMP leads to PKA activation which in turn enhances the release of dense core vesicles containing the neuropeptide NLP-3. PKA may also contribute to Ca^{2+} buffering by activation of the Na^{+}/Ca^{2+} exchanger or to the hyperpolarization of the plasma membrane by activation of K^{+} channels. The lack of CLH-1 in AMsh glia leads to higher levels of $[Ca^{2+}]_i$ (caused by lack of hyperpolarization), hence, to a higher release of glutamate and inhibition of ACY-1, which in turn decreases NLP-3 release. Knockout of *clh-1* may also directly decrease ACY-1 activity. Blue arrows indicate activation. Red lines indicate inhibition. Black arrows indicate transport of ions across the channels. Dashed labels and lines indicate suggested proteins and pathways. Ions and GABA legends are indicated in the figure.

Author Manuscript

Author Manuscript

Author Manuscript

KEY RESOURCES TABLE

REAGENT or RESOURCE	SOURCE	IDENTIFIER
Bacterial and virus strains		
Escherichia coli	CGC	OP50
Chemicals, peptides, and recombinant proteins		
1-octanol	Sigma-Aldrich	Cat#112615
Glycerol	Sigma-Aldrich	Cat#G5516
Isoamyl alcohol	Sigma-Aldrich	Cat#AX1440
Na-acetate	Sigma-Aldrich	Cat#S2889
Diacetyl	Sigma-Aldrich	Cat#B0682
Ethyl alcohol	Pharmco	Cat#111000200
Chloroform	Sigma-Aldrich	Cat#C2432
Dimethyl sulfoxide	Sigma-Aldrich	Cat#D5879
Bicuculline	VWR	Cat#TBC1890
Forskolin	VWR	Cat#102987-308
Gluture	Fisher Scientific	Cat#NC0632797
Experimental models: Organisms/strains		
N_2	CGC (Brenner, 1974)	N2
clh-1(syb2417)	This study (Sunybiotech)	PHX-2417
clh-1(syb2417); blcEx476[pT02B11.3::GFP1-10; pSra-6::RFP]	This study	BLC453
deg-1(u38u421)	CGC (Hart et al., 1999)	TU38
trpa-1(ok999)	CGC (Consortium, 2012)	RB1052
clh-1(ok658)	CGC (Consortium, 2012)	RB833
blcEx319[pT02B11.3::pGM87; pT02B11.3::clh-1 RNAi; Punc-122::GFP]	This study	BLC315
clh-1(ok658); blcEx410[pT02B11.3::clh-1(cDNA); pT02B11.3::pGM87; Punc-122::GFP]	(Grant et al., 2015)	BLC303
clh-1(ok658); blcEx473[pSra-6::clh-1 (cDNA); pSra-6::GCaMP-6s]	This study	BLC447
osm-9 (ky10)	CGC (Colbert and Bargmann, 1995)	CX10
tax-2 (p691)	CGC (Komatsu et al., 1996)	PR691
kyIs39[sra-6::GFP + lin-15(+)]	CGC (Troemel et al., 1995)	CX3465
clh-1(ok658); kyIs39 [psra-6::GFP + lin-15(+)]	This study	BLC319
odr-3 (n2150)	CGC (Colbert and Bargmann, 1995)	CX2205
blcEx446[Psra-6::GCaMP-6s; Punc-122::GFP]	This study	BLC401
clh-1(ok658); blcEx446[pSra-6::GCaMP-6s; Punc-122::GFP]	This study	BLC454
clh-1(ok658); blcEx477[pT02B11.3::clh-1 (cDNA); pSra-6::GCaMP-6s]	This study	BLC455
deg-1(u38u421); blcEx469[pSra-6::GCaMP-6s; Punc-122::GFP]	This study	BLC441

REAGENT or RESOURCE	SOURCE	IDENTIFIER
trpa-1(ok999); blcEx478[pSra-6::GCaMP-6s; Punc-122::GFP]	This study	BLC456
blcEx447[pT02B11.3::GCaMP-6s; Punc-122::GFP]	This study	BLC402
clh-1(ok658); blcEx447[pT02B11.3::GCaMP-6s; Punc-122::GFP]	This study	BLC469
lite-1(ce314); unc-25(e156); kanIs6[Pvap-1::frt2::CoChR::sl2e::TagRFP; pT02B11.3::Flp; pSra-6::GCaMP5.0; Plin44::mCherry]	(Duan et al., 2020)	ST2499
kanIs6; lite-1(ce314); kanEx644[Psra-6::lgc-38 RNAi ; Punc-122::GFP]	(Duan et al., 2020)	ST2181
clh-3(ok763)	CGC (Consortium, 2012)	RB900
clh-3(ok763); clh-1(ok658)	This study	BLC375
clh-1(ok658); Ex[pT02B11.3::clh-3b; Punc-122::GFP]	This study	BLC448
clh-1(ok658); blcEx474[pT02B11.3::rCLC-2 (cDNA); pT02B11.3::pGM87]	This study	BLC328
blcEx53[pT02B11.3::pGM87]	(Grant et al., 2015)	BLC44
clh-1(ok658); blcEx53[pT02B11.3::pGM87]	(Grant et al., 2015)	BLC295
pde-1(nj57); pde-5(nj49); pde-3(nj59); pde-2(tm3098)	CGC (Liu et al., 2010)	TQ1828
pde-1(nj57); pde-5(nj49); pde-3(nj59); pde-2(tm3098); blcEx402[pT02B11.3::clh-1 RNAi; Punc-122::GFP]	This study	BLC371
pde-4(ce268)	CGC (Charlie et al., 2006)	KG744
pde-4(ce268) II; blcEx421[PT02B11.3::clh-1 RNAi; Punc-122::GFP]	This study	BLC449
pde-4(ce268); clh-1(ok658); blcEx446[pSra-6::GCaMP-6s; Punc-122::GFP]	This study	BLC450
pde-4(ce268); deg-1(u38u421)	This study	BLC444
acy-1(md1756)	CGC (Schade et al., 2005)	KG522
clh-1(ok658); acy-1(md1756); blcEx446[pSra-6::GCaMP-6s; Punc-122::GFP]	This study	BLC451
acy-1(md1756); deg-1(u38u421)	This study	BLC435
nlp-3(ok2688)	CGC (Consortium, 2012)	RB2030
pde-4(ce268); blcEx446[pSra-6::GCaMP-6s; Punc-122::GFP]	This study	BLC457
acy-1(md1756); blcEx446[pSra-6::GCaMP-6s; Punc-122::GFP]	This study	BLC458
blcEx361[pT02B11.3::twk-33 RNAi; Pvap-1::RFP]	This study	BLC338
clh-1(ok658); blcEx479[Pvap-1::clh-1 (cDNA); Punc-122::GFP]	This study	BLC496
clh-1(ok658); blcEx480[Psra-6::clh-1 RNAi; Punc-122::GFP]	This study	BLC497
blcEx481[pT02B11.3::Superclomeleon]	This study	BLC498
clh-1(ok658); blcEx481[pT02B11.3::Superclomeleon]	This study	BLC499
blcEx482[pT02B11.3::unc-25 RNAi; Psra-6::GCaMP-6s; Punc-122::GFP]	This study	BLC500
clh-1(ok658); blcEx483[Psra-6::lgc-38 RNAi; Psra-6::GCaMP-6s; Punc-122::GFP]	This study	BLC501
blcEx484[Psra-6::pde-4; Punc-122:GFP]	This study	BLC502
blcEx485[Psra-6::nlp-3 RNAi; Punc-122::GFP]	This study	BLC503

REAGENT or RESOURCE	SOURCE	IDENTIFIER
clh-1(ok658); blcEx486[Psra-6::eat-4 RNAi; Punc-122:GFP]	This study	BLC504
blcEx487[Psra-6::eat-4; Punc-122::GFP]	This study	BLC505
clh-1(ok658); blcEx488[Pnpr-9::glr-5 RNAi; Punc-122::GFP]	This study	BLC506
kcc-3(ok228)	CGC (Consortium, 2012)	RB688
clh-1(ok658); blcEx482[pT02B11.3::unc-25 RNAi; Psra-6::GCaMP-6s; Punc-122::GFP]	This study	BLC507
Oligonucleotides		
pPD95_75	A gift from Andrew Fire	RRID:Addgene_1494
pPD_Pnpr-4::G-CaMP6s	(Hori et al., 2018)	RRID:Addgene_117423
pSH87(Pflp-13::gfp1-10)	(He et al., 2019)	RRID:Addgene_127705
Additional oligonucleotides	Table S2	N/A
Software and algorithms		
Fiji (ImageJ)	NIH	http://fiji.sc RRID:SCR_002285
Micro-manager	Vale Lab, UCSF	https://micro-manager.org/ RRID:SCR_000415
Clampfit	Molecular Devices	http://www.moleculardevices.com/products/software/pclamp.html RRID:SCR_011323
GraphPad Prism	GraphPad software	http://www.graphpad.com/ RRID:SCR_002798
Biorender	BioRender	http://biorender.com RRID:SCR_018361